We thank the associate editor for helping us to improve the manuscript. In this document we provide the author's response to the referees and the marked up version of the manuscript.

Referee 1

The manuscript presents a study on tide-influenced bifurcations based on morphodynamic modelling. The modelling is carried out for a schematized bifurcation and aims to understand tides influence the morphological development of bifurcations. This is an important subject and the conclusions are relevant for understanding the morphological development of tide-influenced deltas. I support publication of the manuscript after moderate revision.

We thank the Referee for his time to read the paper. It helped us to improve the manuscript.

1. **Comment from referee:**

   I think that the manuscript can be improved by presenting more thorough analysis of the model results. The additional analysis should take away the vagueness in the conclusions, like those formulated in the abstract:

   • Line 18-19.

   "…our results show that bedload tends to divide less asymmetrical compared to suspended load, showing a possible stabilizing effect of lateral bed slopes on morphological evolution." The word "possible" suggest that the authors are not sure about this. Better analysis of the model results should clarify this.

   Author's response:

   We agree that "possible" is too weakly formulated. We already know that a lateral bed slope has a stabilizing effect for a bifurcation (Bolla Pittaluga et al., 2003). They showed that the lateral bed slope only affects the bedload transport, causing additional transport of sediment towards the deeper channel. Such a compensating mechanism is not present for suspended load transport. Bedload tend to divide less asymmetric than suspended load as we have shown in the manuscript in Figure 11a below, also because suspended load has a stronger dependence on flow velocity than bed load transport.

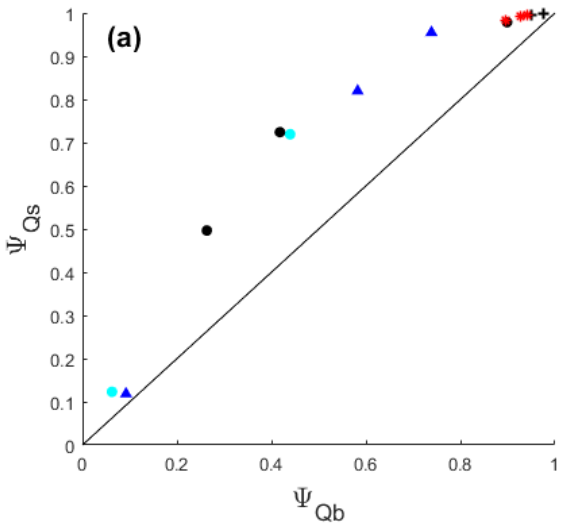

Figure 11a from the manuscript. Comparison of suspended load asymmetry ($\Psi_{susp\ load}$) against bedload asymmetry ($\Psi_{bedload}$) overlaid by the line of equality (black line),

Author's changes in manuscript:

In the abstract of the revised version we removed the word “possible” to be more clear. The previous statement:

“…our results show that bedload tends to divide less asymmetrical compared to suspended load, showing a possible stabilizing effect of lateral bed slopes on morphological evolution.”

Our improvement is in Line 18-20 (Line 18-20 in the marked up version below) as follows:

“…our results show that bedload tends to divide less asymmetrical compared to suspended load and confirm the stabilizing effect of lateral bed slopes on morphological evolution as was also found in previous studies.”

2. **Comment from referee:**

• Line 19-20. “In our simulations, the more tide-dominated systems tend to have a larger ratio of bedload and suspended load transport.” How should I read this? Is this a general conclusion, or is it just because of some special feature in your simulations? In the last case it is not worthy to mention in the abstract, unless it gives explanation to the other conclusions. Otherwise you need to give the physical mechanisms explaining it.

Author’s response:

According to our simulations with different asymmetry in geometry and tides, we have a consistent behaviour where a larger ratio of bedload and suspended load transport occurs in the more tide-dominated condition as given in Fig. 11c below. This is because the tide-river interaction causes a long period of weak flows in one tidal cycle, the strongest flow occurs during ebb tides at which the suspended load transport is the highest. Since river discharge dampens the tides, the low sediment mobility condition which favour bedload transport occurs for a relatively long period, which is during flood and during transition between ebb and flood tides.

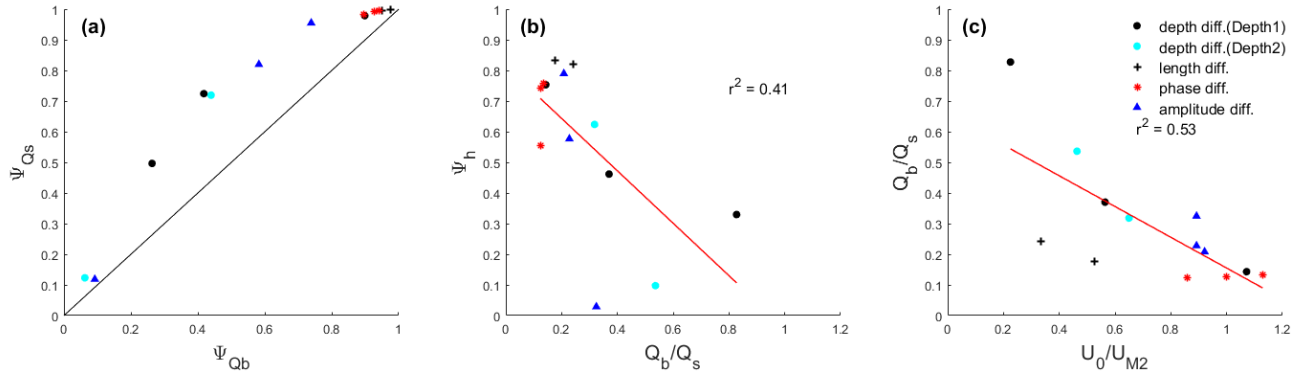

Figure 11 from the manuscript. Comparison of: (a) Suspended load asymmetry ($\Psi_{susp\ load}$) against bedload asymmetry ($\Psi_{bedload}$) overlaid by the line of equality (black line), (b) Scatter plot of morphology asymmetry (Ψ_h) against ratio of bedload and suspended load transport in the upstream channel, and (c) Scatter plot ratio of bedload and suspended load transport in the upstream channels against the dominance of river flow over tidal flows in the upstream channels. The legend for all panels is provided in panel c.

Author's changes in manuscript:

We added additional explanation in Line 20-21 in the revised version (Line 20-23 in the marked up version below) to clarify this as follows:

"We show that the more tide-dominated systems tend to have a larger ratio of bedload and suspended load transport due to periodical low sediment mobility conditions during a transition between ebb and flood. "

3. Comment from referee:

In the model set-up some of the parameters have been given a fixed value without sufficient motivation: "horizontal eddy viscosity was set to 10 m2s-1", "value of 10 for αbn", "αbs =1" (Line 102-106). Especially αbn is a key parameter influencing the distribution of sediment transport to the two downstream branches. Also the horizontal eddy viscosity may be important for the local flow pattern around the bifurcation. Therefore, I expected some sensitivity analysis on these parameters, or at least some motivation why fixed values for them can be used in the study without influencing the conclusions.

Author's response:

For horizontal eddy viscosity, the chosen value (10 m^2s^{-1}) was chosen because a small value can cause numerical instability in the model near the bifurcation because flow magnitudes and direction quickly change. It does not influence the final results.

Transverse bed slope effects for bedload transport were accounted for by the approach of Ikeda (1982) and we used a value of 10 for α_{bn}. This value is much higher than the default value (1.5) and values suggested by Bolla Pittaluga et al. (2003) (0.3-1) because a small value of this parameter in Delft3D leads to unrealistic and grid size-dependent channel incision (Baar et al., 2019). This is kind of a model artefact. The model 'needs' a diffusive process. Near the mouth of an estuary this can come from waves (Ridderinkhof et al. (2016) used realistic values of α_{bn}). Note that although the value is large, it is well within the range of what others used (e.g. Dissanayake et al., 2009; van der Wegen and Roelvink, 2012; Van Der Wegen and Roelvink, 2008). However, we agree that it is an important parameter and that sensitivity should be studied.

For streamwise bed slope effects the Bagnold (1966) approach was used with a Delft3D default value of α_{bs} =1. In general, this does not have a large impact on modelled bed evolution.

Author's changes in manuscript:

The reasoning for the chosen horizontal eddy viscosity was added in Line 112-114 in the revised version (Line 114-116 in the marked up version). For the transverse bedslope effect, additional reasoning mentioned in the Author's response was added in Line 119-123 (Line 121-125 in the marked up version). To strengthen the argument, we ran an additional simulation that apply the α_{bn} of 1 and compared it with the one we used for all simulations (α_{bn} = 10). Compared simulations had the same settings except for α_{bn} to clearly see the effect of the chosen parameter. The results are shown in the plot of final morphology for the two simulations below. The difference between the results from these simulations was discussed in Line 369-380 (Line 376-387 in the marked up version below) and the figure was shown in Line 583 (Line 601 in the marked up version). For streamwise bedslope, we will mention that we used the default value from Delft3D in Line 123-124 (Line 125-126 in the marked up version).

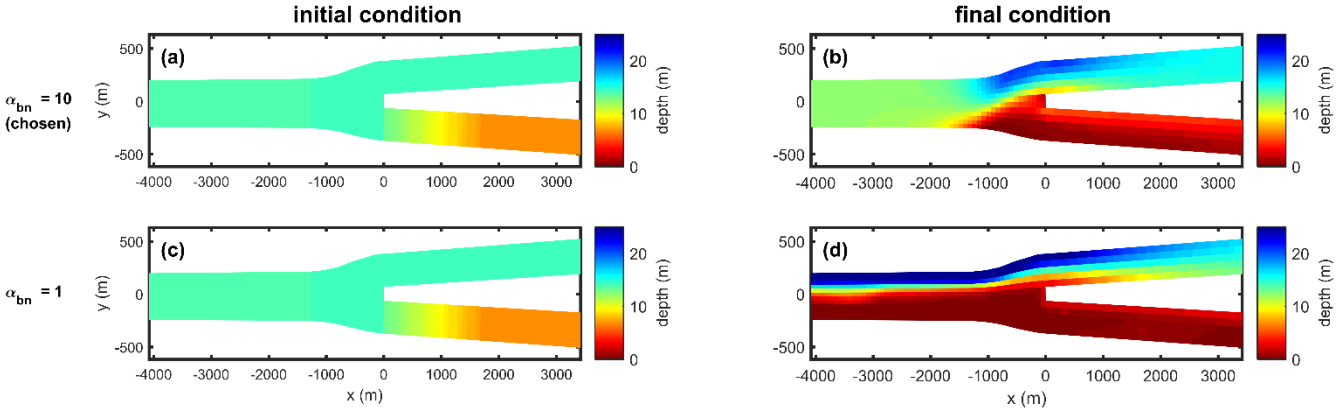

Figure: Initial (left panels) and final (right panels) depth near the bifurcation for different α_{bn}. The same initial and boundary conditions were prescribed as the simulations for the sensitivity of grain size.

4. Comment from referee:

Line 134. "to have Courant Number smaller than 1", why is this needed? I thought that Delft3D uses an implicit scheme.

Author's response:

According to Lesser et al. (2004), Delft3D applies an alternating direction implicit (ADI) to solve the continuity and momentum balance in hydrodynamic simulations. In this scheme one direction is solved implicitly, the other one explicitly. This alternates between time steps. This approach requires a certain courant number for the numerical stability reason (Lesser et al., 2004). Though it has been stated in several papers (e.g. Long et al., 2008; Reyns et al., 2014) that best results are obtained for Courant <1, especially for morphodynamic simulations and system with steep bends, in the Delft3D manual (Version: 3.15.29178, 17 July 2013), it is stated that using ADI scheme the maximum Courant number to fulfil the numerical stability is 4√2 while our model has the maximum Courant number below 1 which fulfil this requirement.

Author's changes in manuscript:

In Line 110-111 in the revised version (Line 112-113 in the marked up version), we mentioned the numerical scheme to solve the shallow water equations. We mentioned the maximum Courant number to fulfil the numerical stability is 4√2 in Line 150-151 (Line 152-153 in the marked up version).

5. **Comment from referee:**

Line 143 & Section 2.2. How about the morphological boundary conditions? What was prescribed at the e.g. the upstream boundary, sediment transport rate or fixed bed?

Author's response:

At inflow condition, the equilibrium sediment transport was prescribed. Thus, the morphology at the open boundaries does not change. During outflow, no boundary condition was needed at the open boundaries and the bed was free to evolve.

Author's changes in manuscript:

We explained morphological boundary condition in Line 154-156 in the revised version (Line 157-159 in the marked up version) as mentioned in the Author's response.

6. **Comment from referee:**

Line 153. Note that even for the largest discharge (2800 m3/s) the velocity at the upstream boundary is only about 0.5 m/s.

Author's response:

Because we built a typical setting for a tidal delta we prescribed a channel with gentle slope ($3x10^{-5}$) (Line 161 in the revised version (Line 164 in the marked up version)). This drives a small river flow. Besides, we also need to prescribe this small river flow to let the tides propagate to the upstream channel and to have conditions in which tidal flows are larger than river flows.

Author's changes in manuscript:

-

7. **Comment from referee:**

Line 178. I do not understand immediately why the first 2 km determines the morphological development of the entire downstream channel.

Author's response:

From our simulations, we found that the development of the downstream channels starts from upstream and develops downstream. Therefore, analysing the most upstream end of the downstream channel is sufficient to determine the growth in asymmetry between them. Based on our simulations, a distance shorter than 2 km cannot be representative to determine the behaviour of the downstream channel (whether they are silting up or deepening) due to the presence of local morphological features near the bifurcation such as bar formation or small incisions in the downstream channel that is silting up. However, a longer distance cannot be representative to determine the downstream channel asymmetry or avulsion because even though one downstream channel almost avulses upstream, tides can cause a deepening near the downstream boundary as

shown in length difference scenario as shown in Figure 5c and f and phase difference scenario in figure 7e and h provided below. Hence, we decided to use the average bed level first 2 km as a representative depth.

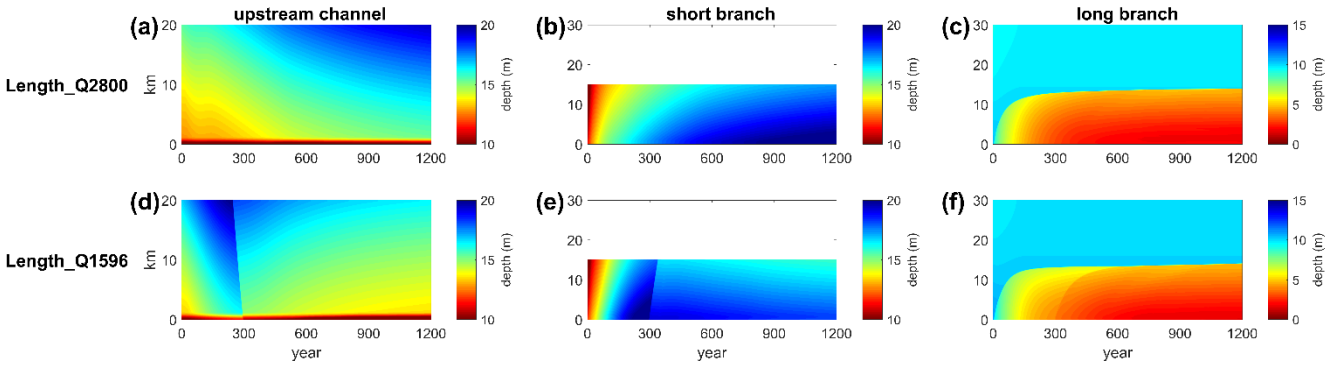

Figure 5 from the manuscript. Time-stack diagram of width- and tide-averaged depth as a function of space for the simulations in Length difference scenario with the same order as Figure 4 but with short (panel (b) and (e)) and long (panel (c) and (f)) downstream branch.

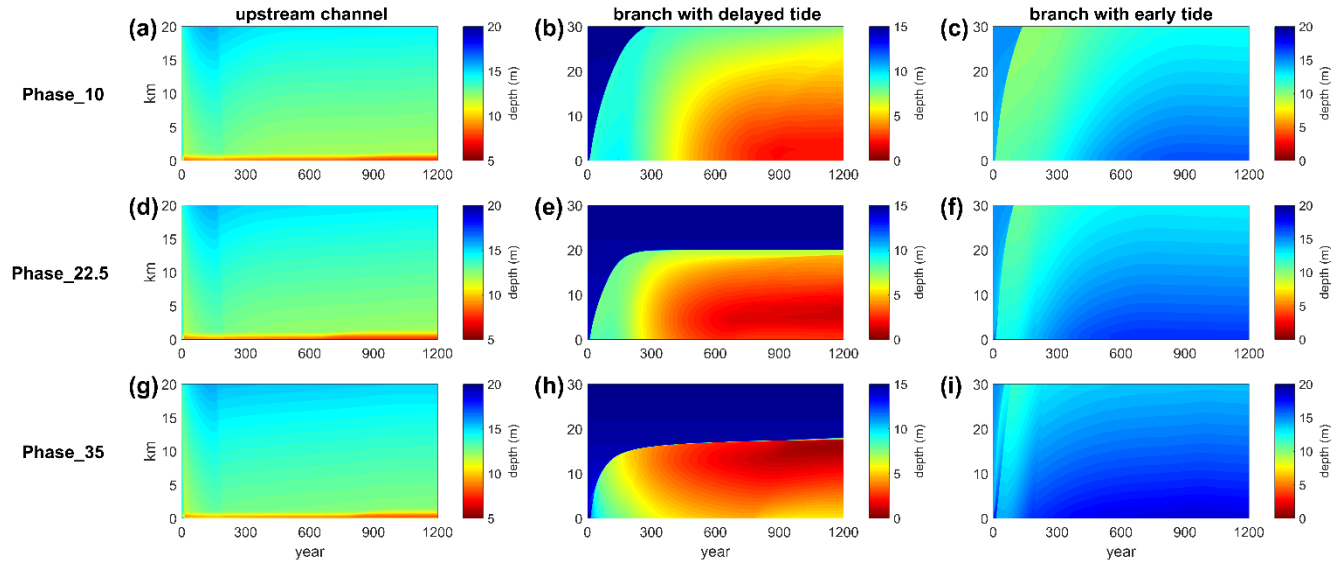

Figure 7 from the manuscript. Time-stack diagram of width- and tide-averaged depth as a function of space for Phase difference scenario.

Author's changes in manuscript:

We explained our motivation to use the first 2 km in Line 197-204 in the new manuscript (Line 201-207 in the marked up version).

8. Comment from referee:

Line 211. “but the depth of the two downstream channels does not depend on the discharge”, this is remarkable. I wonder if this is not because of the short simulation time. Influence of the upstream boundary not yet reached to the downstream branches?

Author’s response:

The statement in line 211 is describing the depth of the two control simulations namely Control_Q2800 and Control_Q1596 which is named according on the prescribed discharge upstream and are with 1 m tidal amplitude at the downstream boundaries. The morphology of the two downstream channels still depends on the prescribed discharge. However, the difference between those simulations is small as shown in time-stack figure below

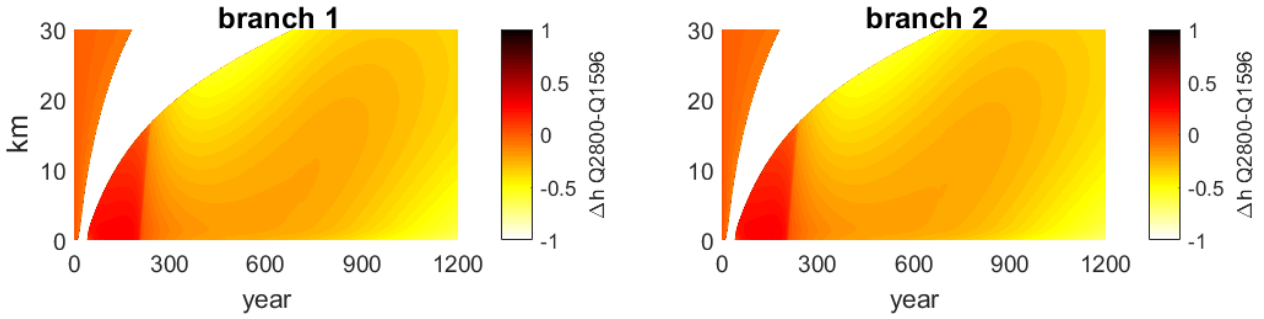

Figure above is time-stack figure of the difference between the depth of simulation Control_Q2800 and Control_Q1596 in branch 1 (left) and branch 2 (right). Negative value means simulation Control_Q1596 is deeper than Control_Q2800. The depth from simulation Control_Q1596 at the end of the simulation is slightly deeper at the end of the simulation period. Here I also provide Figure 3 (the depth from the two compared simulations) from the manuscript.

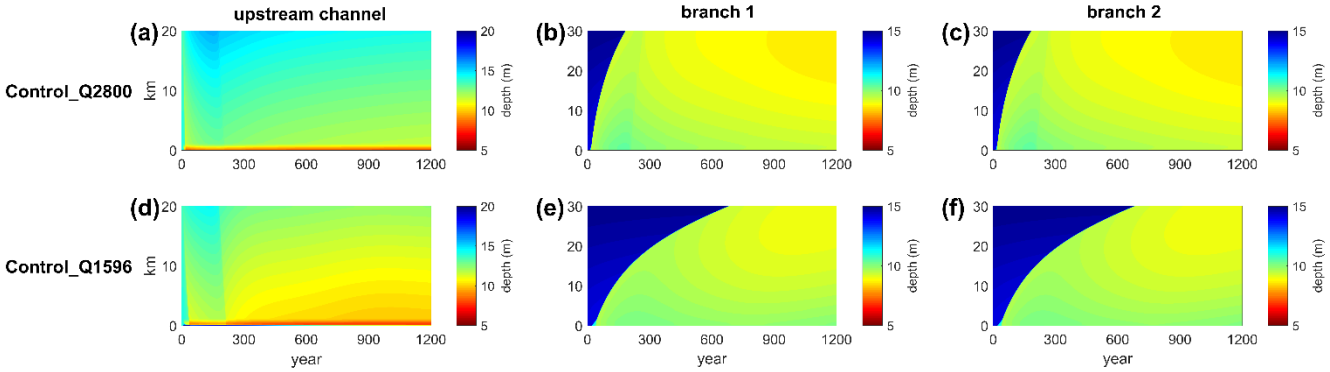

Figure 3 from the manuscript. Time-stack diagram of width- and tide-averaged depth (colour) of the upstream channel (left panels; km 0 is junction, km 20 upstream) and downstream channels (middle and right panels; km 0 is junction, km 30 near sea) as a function of distance from the bifurcation (vertical axis) for the two control simulations. The top panels ((a), (b), and (c)) are the result from the high discharge simulation (Control_Q2800) while the bottom panels ((d), (e), and (f)) are for the low discharge simulation (Control_Q1596).

This small difference in the downstream channel between the two control simulations is because a strong influence of tides in the downstream channels in controlling the morphology. Though river discharge dampens the tides, the widening channel aids to maintain the tidal flow upstream in both downstream channels and causes river-induced flow velocities to become small. Since the two simulations are imposed by the same tidal amplitude, a similar morphology occurs in the downstream channels for both simulations

Author's changes in manuscript:

In the previous version we stated: “but the depth of the two downstream channels does not depend on the discharge”.

In Line 238-240 in the revised version (Line 241-243 in the marked up version) we clarified it:

“...but the depth of the two downstream channels does not significantly affect the depth of the two downstream channels. This is because both control simulations were imposed by the same tidal forcing and the morphology of the downstream channels is mainly controlled by the tides.”

Details:

9. **Comment from referee:**

Line 183. Change “duration of simulations” to “simulated period”?

Line 192. “m3” should be “m-3”.

Author’s response and changes in manuscript:

We improved them in the revised version based on these comments (Line 208 and Line 217 in the revised version (Line 211-220 in the marked up version), respectively).

Referee 2

This manuscript describes a modeling study that seeks to understand morphodynamic adjustments to bifurcations that occur due to river and tide interaction. A novel set of boundary conditions is used. The key finding is that as tidal forcing or tidal heterogeneity (the use phase lags) increases, the stability or symmetry of the bifurcation increases through adjustments to the sediment bed. The straightforward modeling approach affords a relatively clear view of the controlling processes. It is well written, and a solid improvement to our understanding of river delta networks.

We thank the Referee for his time to carefully read the manuscript and for his comments that helped us improving the manuscript.

1. **Comment from referee:**

   One important question I have after digesting this manuscript is the following (the subject heading): The explanation of flow regulation is that the tidal flow from the bigger channel pushes flow into the smaller channel (L289, reason one). This sounds like a rising tide phenomenon, where an incoming tidal waves hits the bifurcation from downstream. However, this is probably a relatively low shear stress and sediment transport moment as the tide fights with the river. The paper states that the most symmetric shields stresses occur at peak ebb flow (L264). At this time, I would expect a falling tide in a deeper channel would pull more water and be more asymmetric. Perhaps this could be elucidated with a Psi_tau*max plot over a tidal period? It would help me understand this key aspect of the system.

   Author's response:

   To clarify, in line 264 in the previous version, Ψ_{τ^*max} is the difference/asymmetry between the maximum peak Shields stress in the two downstream channels (which does not necessarily occur at the same time). This parameter has the strongest correlation with the asymmetry of the final depth between downstream channels.

   We also plotted the Ψ_{τ^*} as a function of time for one of the simulations (simulation Depth1_Q500). If we compare the asymmetry during ebb and flood tides, we agree that the asymmetry during ebb tides is larger than during flood tides. However, the highest asymmetry occurs during the transition between ebb and flood as shown in Figure A below. Compared to this transition condition, the asymmetry during ebb tides is much smaller, even though flow velocities and the absolute difference between the two channels are largest. So, the relative difference decreases although the absolute difference increases. This also explains why for largest tidal influence the relative difference of the Shields stress is smallest. Furthermore, during flood tides the sediment mobility in the downstream channels is relatively small and sometimes close to the critical threshold of sediment motion. It means that during flood almost no sediment is transported. For the simulations with higher discharge (2800 and 1596 m^3s^{-1}) the sediment mobility during flood tides is below the critical threshold of sediment motion indicating no sediment transport.

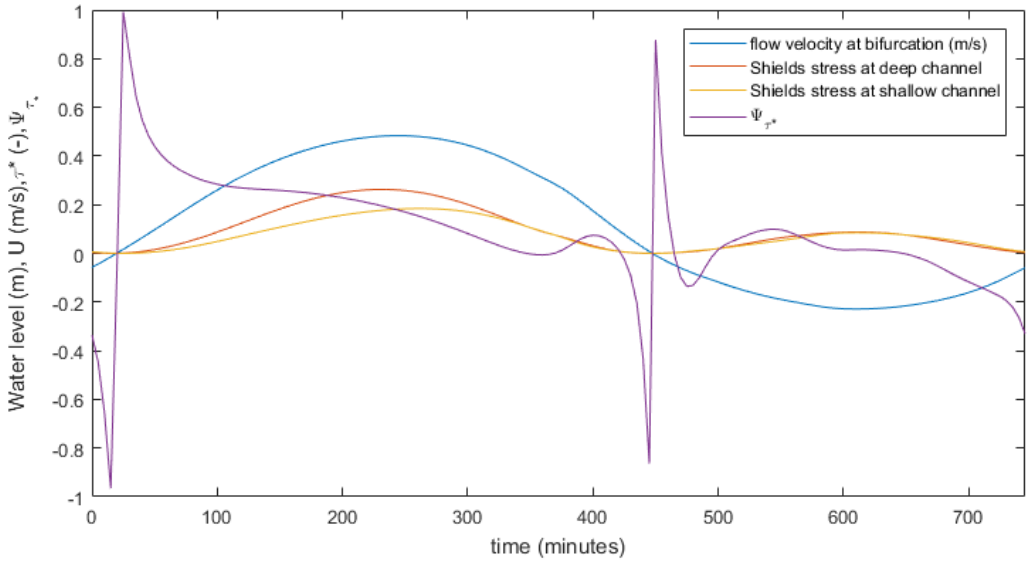

Figure A: Flow velocity in the upstream channel two grids away from the junction (160 m) (blue line), and Shields stress in deep channel (red line) and shallow channel (yellow line) located near the bifurcation (160 m or two grids away) for simulation Depth1_Q500 (simulation imposed by depth difference between branches) overlaid by $\Psi_{\tau*}$ in time. The positive flow indicates ebb flow while negative is flood flow.

Author's changes in manuscript:

-

2. Comment from referee:

Figure 8-11 show correlations of various strength between asymmetry and modeling runs. I am quite surprised by the scatter for example in Fig. 9. With a model that is so simply designed, I would like to know where the scatter comes from. Even if the authors suspect is from numerical errors, it would be good to know. The authors' intuition for this is far better than mine (or the average reader). No information was given about initial bed elevation or bed slope, which seems like an important boundary condition for tidal waves and backwater dynamics. If the system was initialized with a uniform elevation, that information will suffice. Modeling 0.25 mm sediment (L104) in a large tidal system seems too large to be characteristic of tidal systems. I am not suggesting to redo the modeling, but can you justify this choice further?

Author's response:

The scatter in Fig 9 is because we use 5 asymmetry conditions: Depth1, Depth2, Length difference, tidal amplitude and phase difference. Most simulations started out of equilibrium because we do not know the morphodynamic equilibrium for these conditions. We picked these different scenarios to analyse how these types of imposed asymmetry, which is typically found in tidal deltas, will affect the morphodynamic evolution of the bifurcations. Even though we successfully found that they have a similar behaviour, i.e. more tidal influence drives a less morphological asymmetry between downstream channels, the quantity of the morphological asymmetry is different with different imposed asymmetry conditions. With changing morphology, the hydrodynamics also changed. So we did not have full control on where the system would finally end. Besides, not all simulations really reached morphological equilibrium. Though the

morphological change of all simulations at the end of the simulation is small, the morphological change in some simulations still develops very slowly.

Regarding, the channel slope, we have provided the streamwise channel slope ($3x10^{-5}$) in previous version (line 142). Also, we provided the initial depth of all channels in Table 1.

Regarding the grain size, since we are interested in the effect of tides on the asymmetry of the bifurcation for different forcing conditions, we used a single value for the grain size. Thus, we chose a value representative for both more river- and more tide-dominated conditions. Medium sand is a good choice as it is also observed in some deltas such as in Berau River Delta (0.125-0.25 mm) (Buschman et al., 2013), Kapuas Delta (0.22-0.3 mm) (Kästner et al., 2017), Mahakam Delta (0.25-0.4 mm) (Sassi et al., 2011), Mekong Delta (0.074-0.385 mm) (Stephens et al., 2017). However, we do agree that there is no single D_{50} in a system and it differs between systems. The grain size influences the sediment transport mechanisms (bedload versus suspended load) and thereby effect the morphodynamics as shown in the figure below. Therefore, we will study the sensitivity of the model results to the value of d_{50}.

Author's changes in manuscript:

The scatter result in Figure 9 was further explained as mentioned in Author's response in in Line 318-322 in the revised version of the manuscript (Line 322-326 in the marked up version).

We motivated our choice of grain size as discussed above in Line 115-118 (Line 117-120 in the marked up version).

In Line 361-367 in the revised version (Line 368-374 in the marked up version), we discussed model results from a simulation with coarser grain size (0.5 mm) and from finer grain size (0.1 mm) using the same settings, asymmetry condition, and forcing as for the Depth1_Q2800 simulation (Table 1). These additional simulations showed how the model results were affected by the different type of grain size as shown below. Coarser sediment causes the morphology to be less asymmetric, because of the stabilizing effect of the lateral bed slope effect.

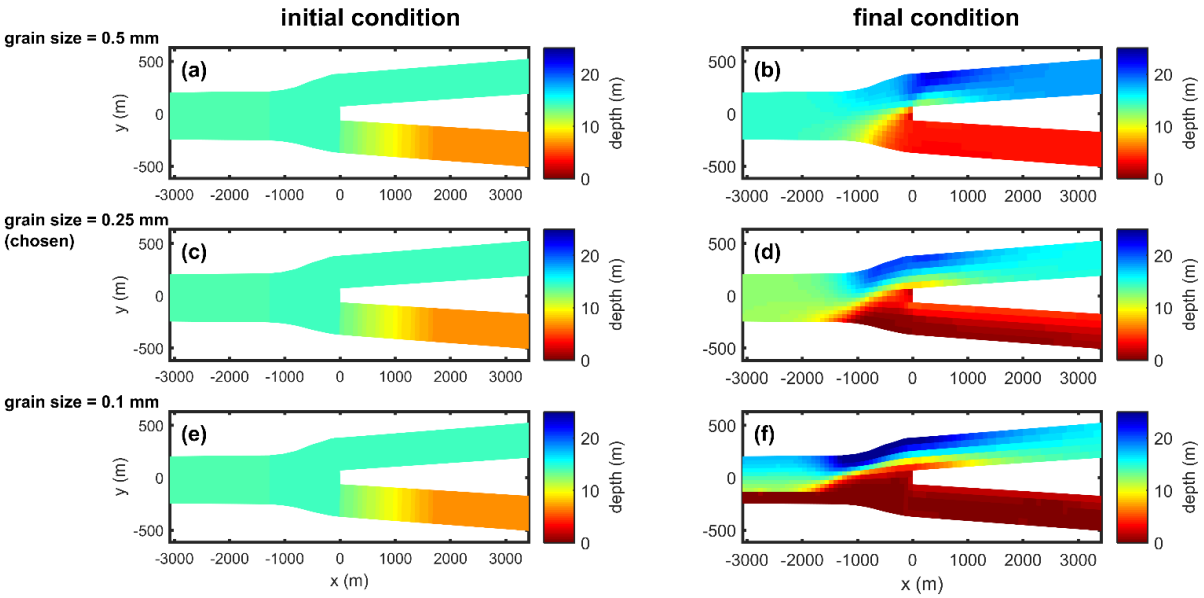

Figure B: Initial (left panels) and final (right panels) depth near the bifurcation for different prescribed grain size. Depth difference between downstream channels was prescribed. One downstream channel has a depth of 7.5 while the other channels were 15 m. At the upstream boundary the river discharge was 2800 m^3s^{-1}. At the downstream boundaries, M_2 tides were prescribed with the amplitude of 1 m.

3. Comment from referee:

Minor Comments L110 I appreciate the discussion of the limitation of the non-adjustible widths. I think it is a reasonable simplifying assumption for this study though. L124 within 800 m of L152-153 over 2km is redundant L166 It took some effort to figure out what eta_i means. I found it in figure 1, but perhaps it could also be explicitly defined in the text here.

Author's response:

The statement in Line 124 was about the width of the channels while the statement in line 152-153 is about the distance where the depth is gradually changing in the shallow downstream channel from the default depth (15 m) to 7.5 m for the first depth difference scenario (Depth1 in table 1). This depth change is gradual to avoid a sudden depth change that may affect the local flow condition.

Author's changes in manuscript:

We explained what eta_1 and eta_2 mean in Line 187-188 in the revised version (Line 190-191 in the marked up version) of the manuscript.

4. Comment from referee:

L234 The Chezy friction factor was set to be constant, so I do not see how differing friction could matter here. Varying depth and the associated reduction in tidal wave celerity is a much more intuitive explanation here.

Author's response:

Indeed, Chézy is the same for both channels, but the friction force is not because it depends on flow velocity as well. Due to the difference in depth the importance of the friction will be also

different in both channels resulting in the different results. That is what we mean in the previous version. We will clarify this in the new version.

Author's changes in manuscript:

We clarified this reasoning in Line 262-264 in the revised version (Line 265-267 in the marked up version) as follows:

"Because the depth in the channels influences the tidal dynamics (by for example the relative importance of friction and by difference in tidal propagation speed due to the different initial depths), the tide-induced flows were different at the junction and stayed different during the entire simulation."

5. **Comment from referee:**

L289 Processes instead of reasons? L326 Findings L351 asymmetrically L354 "relatively ratio" a word is missing here.

Author's response and changes in manuscript:

We modified them according to this comment in Line 324, Line 382, Line 407, and Line 409, respectively (Line 328, 389, 415, 417 in the marked up version).

6. **Comment from referee:**

Figure 2-7. The size and colormaps make these figures very difficult to gather information from. I recommend either adding 2-4 contours to the plots or just using 2-4 colors instead of a spectrum. Basically all of the detail in plots like Figures like Fig7a can't be seen by the reader.

Author's response:

We changed the colormap into 4 colour contour which is more clearly for the reader to see the deepening and shallowing

Author's changes in manuscript:

The colormap of Figure 3-7 was changed with four colour contour in Line 542, 548, 553, 557, and 560 in the revised manuscript (Line 553, 560, 566, 571, 575 in the marked up version). The example of improved Figure 4 (the time-stack of one of the scenario (depth difference 1)) is shown below.

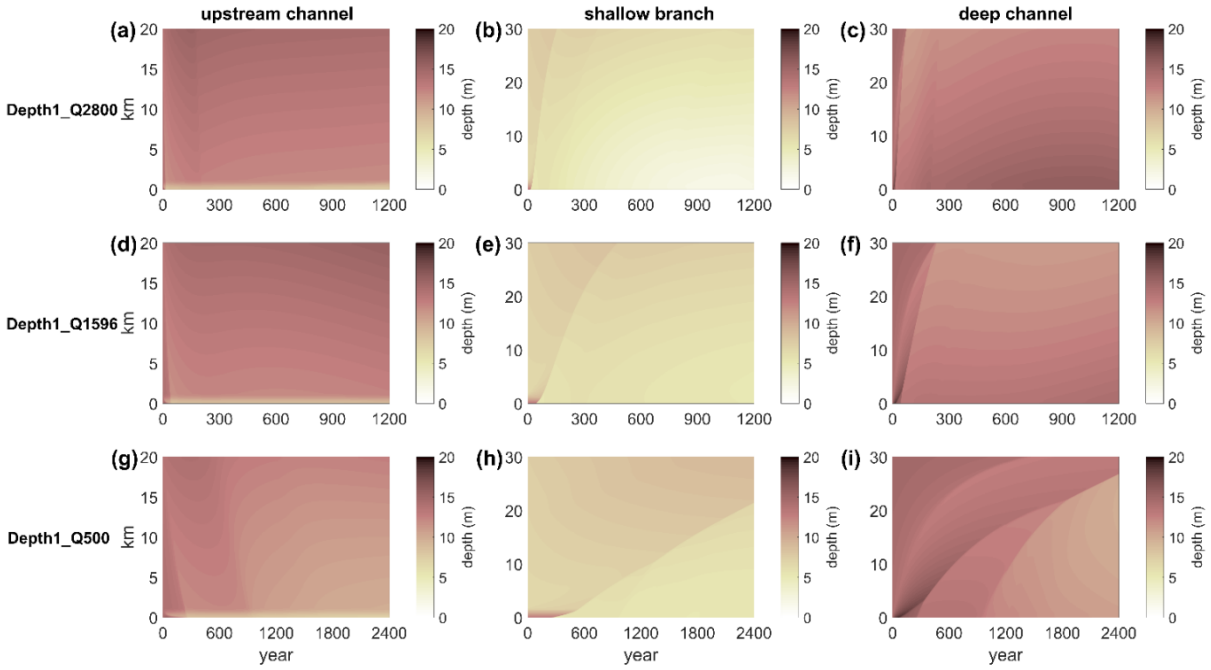

Figure C: Same plot as Figure 3 but for simulations of Depth1. The panels from top to bottom show the results from different simulation (Depth1_Q2800, Depth1_Q1596, Depth1_Q500, respectively) while from left to right show the upstream channel, shallow branch, and deep branch, respectively. Different scale of colour bar for different channel is applied.

Referee 3 (spesific comments)

We thank the Referee for his time to carefully read the manuscript and for his comments that helped us improving the manuscript.

1. **Comment from referee:**

   1) I think the authors should take more in consideration some of the recent theoretical

   results.

   The analytical model of Redolfi et al. (2016), which represents a fully two-dimensional extension of the Bolla Pittaluga et al. (2003, 2015) model, has been proven to effectively predict the stability of both gravel and sand bed bifurcation (Redolfi et al. 2019) with the key advantage of avoiding the calibration of a specific parameter (like the α parameter of Bolla Pittaluga el al., 2003). I think these recent advancements should be at least mentioned in the Introduction and/or in the Discussion (Section 4.2).

   Similarly, in the work of Salter et al. (2017) which specifically focuses on the effect of downstream conditions on the bifurcation stability, should be considered in the Introduction.

   Please ignore this comment if you think it is too personal (I am the main author of the above-mentioned papers).

   Author's response:

   We agree that the mentioned work is a good extension of the work of Bolla Pittaluga et al (2003; 2015), although the fundamentals are still the same. Furthermore, we are also aware of the work of Salter et al. (2017).

   Author's changes in manuscript:

   We added these references in both introduction (Line 57-63) and discussion (Line 394) in the revised version of the manuscript (Line 59-65 and 401-402 in the marked up version). We did not fully compare out model results with the mentioned papers because by using a 2DH model we don't need a nodal point relation.

2. **Comment from referee:**

   2) Line 52: this sentence is misleading, as Bolla Pittaluga et al. (2003) did not test the effect of meandering bends. 3) Line 97: the sentence "the 2D approach also results in reliable morphodynamic simulations" is very vague, as the reliability of depth-averaged models clearly depends on the specific problem under consideration.

   Author's response:

   Line 52: We agree that the text is not very clear in the previous version. We meant that the transverse channel slope, as studied by Kleinhans et al. (2008), was similar as in Bolla Pittaluga et al. (2003). However, Kleinhans et al. (2008) added the effect of meandering upstream channel in the transverse transport calculation.

   Line 97: Since in this study we are interested to investigate a large scale morphological development, simulating a detail 3D result is not our goal. Therefore, 2D model is sufficient and can reduce the computational cost.

Author's changes in manuscript:

We removed the citation to Bolla Pittaluga et al. (2003) for this sentence to avoid misunderstanding (sentence in Line 53-54 in the revised version of the manuscript (Line 55-56 in the marked up version)).

In line 101-105 in the revised version (Line 103-107 in the marked up version), we strengthened and elaborated our argument why we chose 2D model instead of 3D according to the reasoning that we mention in the Author response.

3. **Comment from referee:**

4) Section 4.2: it would be useful to provide an indication of the average Shields number.

Author's response:

We agree. We will provide a table of Shields numbers and flow conditions at the bifurcation.

Author's changes in manuscript:

We provided a table that provides the information of: tide averaged Shields number, maximum Shields number, mean flow velocity, and M_2 velocity amplitude at the bifurcation in Line 606-609 in the revised version (Line 624-627 in the marked up version).

4. **Comment from referee:**

5) Code availability: to enable the reproducibility of the results, I recommend the authors to share the configuration files.

Author's response:

We will provide the configuration files for all simulations in the supplement.

Author's changes in manuscript:

The supplement was mentioned in Line 412-413 in the revised version (Line 420-421 in the marked up version).

5. **Comment from referee:**

6) System of coordinates: I cannot see the reason for placing the bifurcation at x=220 km an y∼9 km. What is the meaning of the origin (i.e. x=0, y=0) point? Setting x=0 and y=0 at the bifurcation node would have been more meaningful, and it would have facilitated the reading of the maps.

Author's response:

This coordinate system was due to the way the grid was built in which x=0 is located at the upstream end of upstream channel.

Author's changes in manuscript:

We moved the origin of the x and y coordinate system to the bifurcation, e.g. in Line 532 and 538 in the revised version (Line 541 and 548 in the marked up version).

6. **Comment from referee:**

7) Units: space between value and unit is sometimes missing (e.g., line 177); please also note that units should not appear in italic (Equation 1);

Author's response and changes in manuscript:

The space was added in the new version for all missing space (Line 161, 201, 278, 279, 306) (Line 164, 200, 281,282, 310 in the marked up version). Equation 1 was also fixed (Line 136).

7. **Comment from referee:**

8) Graphics: in several figures (e.g., Figures 7 and 11) the labels are disproportionately small; in Figure A1: the quantities represented on the two axes are "x" and "y", not "x-axis" and "y-axis.

Author's response and changes in manuscript:

The labels and the axes were improved according to this comment in the new version (e.g. Line 542, 548, 581, 585, 592, 598).

Morphological evolution of bifurcations in tide-influenced deltas

Arya P. Iwantoro[1], Maarten van der Vegt[1], Maarten G. Kleinhans[1]

[1] Department of Physical Geography, Faculty of Geosciences, Utrecht University, Utrecht, 3508 TC, The Netherlands

Correspondence to: Arya P. Iwantoro (a.p.iwantoro@uu.nl)

Abstract. In river-dominated deltas, bifurcations often develop an asymmetrical morphology, i.e. one of the downstream channels silts up while the other becomes the dominant one. In tide-influenced systems, bifurcations are thought to be less asymmetric and both downstream channels of the bifurcation remain open. The main aim of this study is to understand how tides influence the morphological development of bifurcations. By using a 2DH morphodynamic model (Delft3D), we simulated the morphological development of tide-influenced bifurcations on millennial time scales. The schematized bifurcation consists of an upstream channel forced by river discharge and two downstream channels forced by tides. Two different cases were examined. In the first case, the downstream channels started with unequal depth or length but had equal tidal forcing, while in the second case the morphology was initially symmetric but the downstream channels were forced with unequal tides. Furthermore, we studied the sensitivity of results to the relative role of river flow and tides. We find that with increasing influence of tides over river, the morphology of the downstream channels becomes less asymmetric. Increasing tidal influence can be achieved by either reduced river flow with respect to the tidal flow, or by asymmetrical tidal forcing of the downstream channels. The main reason for this behaviour is that tidal flows tend to be less unequal than river flows when geometry is asymmetric. For increasing tidal influence, this causes less asymmetric sediment mobility and therefore transport in both downstream channels. Furthermore, our results show that bedload tends to divide less asymmetrical compared to suspended load and confirm the stabilizing effect of lateral bed slopes on morphological evolution as was also found in previous studies.~~, showing a possible stabilizing effect of lateral bed slopes on morphological evolution.~~ We show that the more tide-dominated systems tend to have a larger ratio of bedload and suspended load transport due to periodical low sediment mobility conditions during a transition between ebb and flood.~~In our simulations, the more tide-dominated systems tend to have a larger ratio of bedload and suspended load transport.~~ Our results explain why distributary channel networks deltas with strong tidal influence are more stable than river-dominated ones.

1 Introduction

Deltas often consist of distributary channel networks. In these systems, water and sediment are divided at the bifurcations and distributed over the delta. The shape of the delta and the number of active channels depends on many factors like the forcing by rivers, tides and waves (Galloway, 1975; Rossi et al., 2016; Shaw and Mohrig, 2014), sediment availability and sediment type (Geleynse et al., 2011). Bifurcations tend to develop differently in river- than in tide-dominated systems, because tides

influence the mouth bar formation processes of active river-dominated deltas (Edmonds and Slingerland, 2007; Leonardi et al., 2013; Shaw and Mohrig, 2014). In tidal deltas tides propagate upstream and can induce bi-directional flows. This unique characteristic may lead to a different morphological evolution of the bifurcations than would occur in the river-dominated zone (Frings and Kleinhans, 2008; Hoitink et al., 2017), but this has not been proven yet and the underlying mechanisms have not been studied. The focus of this paper is on the stability and depth asymmetry of bifurcations in tidally influenced deltas. We do not focus on the morphological evolution of the entire delta or the formation process of mouth bars, but consider a single bifurcation consisting of one upstream and two downstream channels. These are the building blocks of deltas and the hydro- and morphodynamics of such a system has been studied before by many others (Wang et al. 1995; Bolla Pittaluga et al., 2003; Buschman et al., 2010; Kleinhans et al., 2008; Buschman et al., 2010; Sassi et al., 2011; Buschman et al., 2013).

In river-dominated systems, the morphology of the downstream channels of bifurcations often develops asymmetrically, such that one downstream channel deepens while the other silts up (Kleinhans et al., 2008). In many cases this condition develops into an avulsion. This asymmetric development can be triggered by a small perturbation such as a different bed elevation at the junction (Bolla Pittaluga et al., 2003), by a meandering upstream channel nearby the bifurcation or by the geometry of the downstream channels such as different length of the downstream branches (Kleinhans et al., 2008). The study about this morphological evolution in river-dominated bifurcations was pioneered by Wang et al. (1995). They applied an analytical model to predict the stability of river bifurcations. They found that bifurcations can be stable if any tendency for downstream branch to become more dominant is counteracted by a relatively large share of the sediment input. Bolla Pittaluga et al. (2003) improved the model of Wang et al. (1995) by taking into account the cross-channel flow that can be induced by an asymmetric cross-sectional profile at the bifurcation. This effect induces a lateral bedload transport, which affects the asymmetric sediment division to the downstream branches. Using this approach, they found that the asymmetry of depth of the two downstream branches depends on the Shields number and on the width-to-depth ratio of the upstream channel at the bifurcation. Bifurcations with high width-to-depth ratio and that are dominated by suspended load transport will be instable and develop asymmetrical depths. Bertoldi and Tubino (2007) confirmed the results of Bolla Pittaluga et al. (2003) using a physical-scale model. Kleinhans et al. (2008) proposed that this asymmetrical depth development is also influenced by meandering of the upstream channel. The meandering bend induces an asymmetrical cross-sectional bed profile ~~as tested by Bolla Pittaluga et al. (2003)~~, and thereby influences the division of sediment at the junction. Bolla Pittaluga et al. (2015) continued the work of Bolla Pittaluga et al. (2003) for a wider range of sediment mobility conditions. They found a range of sediment mobility numbers that result in stable symmetric bifurcations. Meanwhile, bifurcations with sediment mobility higher or lower than this range will grow asymmetrically and avulse. Applying the concept of Bolla Pittaluga et al. (2003), ~~(~~Salter et al.~~,~~ (2017) showed that deposition of sediment at a relative shallow shelf causes the shorter channel to lengthen and reduce in gradient, thereby balancing the sediment transport division between downstream channels with unequal lengths. ~~(~~Redolfi et al.~~,~~ (2016) eliminated the need for a calibrated parameter in the lateral bedload transport of Bolla Pittaluga et al. (2015) and by using that approach, Redolfi et al. (2019) showed that stable, symmetric bifurcations can only occur when the width-to-depth ratio of the

upstream channel is below the critical limit originally defined in the theory of meandering rivers by (Blondeaux and Seminara, (1985) where the critical limit value depends on the friction and Shields stress at bifurcation.

In contrast to our knowledge of morphological development of bifurcations in river-dominated systems, our knowledge of this particular area in tide-influenced systems is still limited. Observations suggest that a similar development as in river-dominated systems can occur, as for example found in the most upstream bifurcation of the Yangtze Estuary that divides the main channel into North Branch and South Branch. According to Chen et al. (1982), the North Branch has evolved to be narrower and shallower while the South Branch has deepened. However, bifurcations in other tide-influenced deltas have downstream channels that seem to have a less asymmetric depth distribution, for example the Berau River Delta (Buschman et al., 2013) and Kapuas River Delta (Kästner et al., 2017). It has been suggested that tidal deltas have more stable distributary channel networks than their river-dominated counterparts (Hoitink et al., 2017), but the underlying mechanisms are unknown. Furthermore, several studies have investigated tidal characteristics at tidal bifurcations. Despite a general understanding on tides and subtidal water division at tidally influenced bifurcations (Buschman et al., 2010; Sassi et al., 2011; Zhang et al, 2012; Buschman et al., 2013; Alebregtse and de Swart, 2016), the effect of tides on the morphological evolution of tidal bifurcations has not been fully understood yet. From previous studies it is clear that tides influence the subtidal flow (Buschman et al., 2010; Sassi et al., 2011) and sediment division (Buschman et al., 2013), induce tidal currents that influence the sediment mobility, and can cause cross-channel currents at the junction (Buschman et al., 2013; Kleinhans et al., 2013). In river systems, all these factors are important for the morphological development of the downstream channels and it is expected that this is also the case for tide-influenced systems.

Therefore, the main aim of this paper is to study the effect of tides on the morphological evolution of bifurcations with the focus on how tides contribute to the asymmetrical development. For this purpose, an idealized bifurcating channel was set-up in Delft3D. We simulated the morphological evolution of a system consisting of two downstream channels (branches) forced by tides and an upstream channel forced by river discharge. We consider this system as a building block of each delta system. We studied two cases, i.e. asymmetric geometry of downstream channels, and asymmetric tides between the downstream channels. In the former case, the asymmetric downstream geometry was initially prescribed to see how tides affect the asymmetrical development of the downstream channels. The relative effect of tides was investigated by imposing equal tides at downstream boundary of each downstream branch and by using different values for the river discharge in a series of simulations. In the latter case, we imposed unequal tidal forcing at the two downstream boundaries that had a symmetric geometry. In tide-influenced deltas, the asymmetric tides between downstream channels can occur because the downstream channels are connected to other channels with different complexity, which may dissipate the tidal range or slow down the tides unequally before the tides propagate into the downstream channels of the bifurcation.

This paper is organized as follows. The model setup and methodology are described in Section 2. In Section 3, the results of the simulated morphological development are presented. Section 4 presents a discussion on the findings. Finally, the conclusions of this study are provided in Section 5.

2 Methodology

2.1 Model set-up

An idealized bifurcating channel was set up and its morphological development was simulated using the depth-averaged version (2DH) of Delft3D. This 2D approach is suitable for long-term and large scale morphodynamic modelling because it is computationally lighter than a 3D approach. Even though a 3D approach allows for vertical flow patterns (Lane et al, 1999) such as curvature induced flow, which might be important for the sediment transport process (Daniel et al., 1999), the 2D approach ~~also results in reliable morphodynamic simulations (Lesser et al., 2004)~~is sufficient for this study since we focus on large -scale morphodynamical evolution and therefore simulating detail 3D features of flow and morphology is not our goal. Furthermore, the reason to prefer the 2D above the 1D approach is to explicitly simulate cross-channel flow induced by tidal propagation from one branch to another at the junction as observed in Buschman et al. (2010) and Buschman et al. (2013) and as being identified by Bolla Pittaluga et al. (2003) as an important process for sediment division at the junction.

The model solved the 2DH unsteady shallow water equations using an semi-implicit Alternating Direction Implicit (ADI) scheme on a staggered grid (see Lesser et al., 2004). For bed friction the Chézy formulation was used with a value of 60 $m^{1/2}s^{-1}$~~,~~. Meanwhile the horizontal eddy viscosity was set to 10 m^2s^{-1}. This value was chosen because applying a smaller value for horizontal eddy viscosity will cause a numerical instability near the bifurcation as flow magnitude and direction rapidly change in this location. Bedload and suspended load sediment transport were calculated by the van Rijn (1993) method. We used medium sand with a single grain size of 0.25 mm with a dry bed density of 1600 kg m^{-3}. This sediment size is in the range of observed grain size in tide-influenced deltas, as for example by Buschman et al. (2013) in Berau River Delta (0.125-0.25 mm), Kästner et al. (2017) in Kapuas Delta (0.22-0.3 mm), Sassi et al. (2011) in Mahakam Delta (0.25-0.4 mm), and ~~(~~Stephens et al.~~,~~ (2017) in Mekong Delta (0.074-0.385 mm). Transverse bed slope effects for bedload transport were accounted for by the approach of Ikeda (1982) and we used a value of 10 for α_{bn}. This value is much higher than Delft3D default value (1.5) and suggested by Bolla Pittaluga et al. (2003) (0.3-1) because a low value of this parameter in Delft3D leads to unrealistic and grid size-dependent channel incision as well as bar formations (Baar et al., 2019). Even though we prescribed a high α_{bn}, this value is still in the range of what other studies used for Delft3D modelling work (e.g. Dissanayake et al., 2009; van der Wegen and Roelvink, 2012; Van Der Wegen and Roelvink, 2008). For streamwise bed slope effects the Bagnold (1966) approach was used with a Delft3D default value of α_{bs} =1. For morphology the MorFac approach was used (Lesser et al., 2004; Roelvink, 2006) with an acceleration factor of 400. We tested several values between 1 and 1000, and chose the largest value for which morphology had similar development as for value of 1 and numerical stability was satisfied. This allows for long-term

morphodynamic simulation at time scales of decades (Lesser et al., 2004) and centuries (van der Wegen et al., 2008) in much shorter duration. Furthermore, in this study, non-erodible channel banks were used. This limitation was acceptable since changes in width-depth ratio could still be accommodated by the bed level change, and using erodible banks is not realistic as long as the model is not able to allow for channel bank growth.

The spatial domain consisted of an upstream channel that bifurcates in two downstream channels. The two downstream channels had a default length of 30 km, although in one series of simulations the length of one channel was 15 km. The upstream channel had a length of 220 km to ensure that upstream propagating tides decay smoothly. The downstream channels and the first 20 km of the upstream channel had a convergent width profile, while the upstream 200 km had a constant width. The channel width was configured by:

$$W_{upstream}(x) = \begin{cases} W_0 e^{-x/L_w}, & \text{for } x < 20 \text{ km} \\ W_0, & \text{for } x > 20 \text{ km} \end{cases},$$

$$W_{downstream}(x) = 0.5 W_0 e^{-x/L_w}, \quad (1)$$

in which W(x) is the channel width, x the longitudinal distance from the junction (i.e. positive in upstream direction, x=0 is at bifurcation, hence negative x in downstream channels), W_0=322 m is the width at the junction and L_w=50 km is the e-folding length scale. Further, in a region within 800 m near the junction an additional widening was applied (panel b in Figure 1) to overcome the loss of two grid cells (see grid description and Kleinhans et al. (2008)). This widening is a typical feature of bifurcations found in delta systems (Kleinhans et al., 2008). After the additional widening, W_0 becomes 750 m.

The spatial domain of the model was discretized in a curvilinear grid and followed the same method as in Kleinhans et al. (2008) and Buschman et al. (2010). At the bifurcation two grid cells had to be removed in the middle of the channel for numerical reasons (Kleinhans et al., 2008), as illustrated in Figure 1. The grid cell length in along channel direction was 80 m. The upstream channel had 12 grid cells across the channel whereas in both downstream channels 5 grid cells were used. Therefore, the grid cell size in across channel direction was spatially varying in order to adapt the funnelling shape of the channel. Near the junction this resulted in typical grid cell width of 40 m. Based on grid size and channel depth a time step of 6 seconds was used in all simulations to have Courant Number smaller than 4√2 as required for the ADI scheme~~1~~. The domain had three open boundaries where boundary conditions for flow and sediment transport were prescribed. At the upstream end of the upstream channel river discharge was prescribed while ~~and equilibrium conditions for sediment transport at inflow. a~~At the ends of the two downstream channels M_2 tidal water levels were imposed ~~and equilibrium sediment transport rates at inflow~~. At all open boundaries, equilibrium sediment transport was computed during inflow while during outflow the sediment transport was assumed to be just flushed out from the domain. As a result, no morphological change occurred during inflow but the bed is free to evolve during outflow.

Because the formation of alternating bars will affect flow and sediment division at the junction, the channel depth and upstream prescribed river discharge were chosen such that the system was in the overdamped bar regime (Struiksma et al., 1985). To this end, we conservatively followed the empirical classification proposed by Kleinhans and van den Berg (2011) . Therefore, the three connected channels had an initial depth of 15 m and a constant along-channel bed slope of $3x10^{-5}$ m m^{-1}. The prescribed discharge was ranged between 500 and 2800 m^3s^{-1}.

2.2 Description of model scenarios and boundary conditions

Depth, width and length of the downstream channels of bifurcations in deltas can be unequal. Hence, in Case 1 we started the simulations with an unequal geometry, either being a difference in depth or length between the two downstream channels. We simulated the morphological evolution of the bifurcation until it approximately reached morphodynamic equilibrium (discussed later on). Note that length of the branches was fixed in time, while an initial depth difference not necessarily results in an asymmetric equilibrium depth because it can adapt. All simulations belonging to Case 1 were forced by equal tides from downstream and river discharge from upstream (settings summarized in Table 1). The depth difference scenarios were performed in two different ways. First, simulations were started from a system in which the upstream channel and one downstream channel were 15 m deep, while the other branch was 7.5 m deep (called Depth1). The upstream 2 km of the shallow downstream channel was gradually changed over 2 km to avoid a sudden depth change near the bifurcation. In a second type of simulation, we started with uniform bathymetry of 15 m depth and simulated till morphodynamic equilibrium was reached (called Depth2). Next, one downstream channel was made 0.5 m deeper and the other 0.5 m shallower. We studied the sensitivity of the results to the relative magnitude of tides over river discharge by changing the prescribed upstream discharge. The simulation with largest river discharge (2800 m^3s^{-1}) represents a river dominated system while the simulations with lower river discharge (500 m^3s^{-1}) represent the more tide-influenced systems.

In Case 2 the effect of unequal tidal forcing on morphological development was studied. In natural systems tides in the two downstream branches can be unequally forced. For example, when the two branches end in a shelf sea, amplitude and phase in the two channels can be different because they have a different position with respect to the amphidromic system in the shelf sea. Furthermore, in deltas with multiple bifurcations and unequal depths and channel lengths, tidal amplitude and phase differences will be present in the channels because propagation speeds and times in the channels are different. Hence, in Case 2 we started simulations with a symmetric geometry but with asymmetric tidal forcing, either being a tidal water level amplitude difference or a tidal phase difference. The corresponding settings of the simulations can be found in Table 1. The difference in downstream tidal forcing between the two channels was studied for values between zero and 0.75 m (η_1 in Figure 1 was 0.75, 0.5 or 0.25 m while η_2 was 1 m) where η_1 and η_2 are tidal water level amplitude imposed at the downstream end of downstream channel 1 and 2, respectively. Mean, while for another set of simulation the tides had equal amplitude but the phase difference was 10, 22.5, or 35 degrees (for M_2 tide this means one channel had delayed tides of 20, 46 or 72 minutes).

We also performed two control simulations (with symmetric geometry and equal tides) to study the equilibrium bed profiles in absence of any initial asymmetry. The morphology change simulated for Case 1 and Case 2 were caused by the asymmetric forcing/geometry and by the adaptation to the initial conditions. Therefore, the results of the control simulations can be used to better interpret the simulations of Case 1 and Case 2.

2.3 Methods to evaluate model simulations

The morphological development of the bifurcation was observed by evaluating for each downstream channel the tidally and spatially averaged depth of the first 2 km from the bifurcation (Figure 2, called h_1 and h_2 from hereon). This region was chosen because it determined the morphological development of the entire downstream channel. The development of the downstream channels starts from upstream and develops downstream. Therefore, analysing the most upstream end of the downstream channels is sufficient to determine the growth in asymmetry between them. After analysing all cases, it was found that a distance shorter than 2 km cannot be representative due to the presence of local morphological features near the bifurcation such as bar formation or small incisions in the downstream channel that is silting up. However, a longer distance cannot be representative because even though one downstream channel almost avulses upstream, tides can cause a deepening of that same channel near the downstream boundary. To determine whether the system was in morphodynamic equilibrium we analysed the evolution in time of h_1 and h_2. We stopped the simulation when the changes in h_1 and h_2 were small. A true morphodynamic equilibrium, in the sense that no bed level change occurred in the entire domain, was never achieved. This is very common for morphodynamic simulations of estuaries (Van Der Wegen and Roelvink, 2008; Nnafie et al., 2018). Typical ~~duration of simulations~~simulated period was between 1200 and 2400 years, depending on the prescribed river discharge.

To compare the depth of the two downstream channels, the depth asymmetry parameter Ψ_h was calculated as:

$$\Psi_h = \frac{|h_2 - h_1|}{h_1 + h_2}. \quad (2)$$

A larger Ψ_h indicates a more asymmetric morphology. When Ψ_h is close to one this indicates an avulsion, given that the widths are fixed, while a zero value indicates equal depth of the downstream channels.

The sediment mobility was evaluated by calculating the width-averaged value of the Shields number two grid cells away from the bifurcation, as illustrated in Figure 2. The Shields number at each grid point was calculated as:

$$\tau_* = \frac{\tau_b}{(\rho_s - \rho_w) g D_{50}}, \quad (3)$$

where $\rho_s - \rho_w$=1650 kg m^{-3}, g is gravitational acceleration (9.81 m^{2}s^{-1}) and τ_b is the bed shear stress magnitude expressed by

$$\tau_b = \frac{\rho_w g u^2}{C^2}, \quad (4)$$

in which C is the Chézy coefficient and u is instantaneous flow velocity. , In tide-influenced systems, tides cause a temporal change of bed shear stress and we calculated both the peak and the tide-averaged value of the Shields number. A Shields asymmetry parameter $\Psi_{\tau*}$ was defined and calculated by:

$$\Psi_{\tau*} = \frac{|\Delta\overline{\tau_{*;1,2}}|}{\overline{\tau_{*,1}}+\overline{\tau_{*,2}}}, \quad (54)$$

where $\overline{\tau_{*,1}}$ and $\overline{\tau_{*,2}}$ are the width-averaged Shields number in each downstream channel and $\Delta\overline{\tau_{*;1,2}}$ is the difference between both. A higher value of $\Psi_{\tau*}$ indicates a more asymmetric sediment mobility condition while Ψ_{τ}=0 indicates a symmetric sediment mobility. When $\Psi_{\tau*}$ was based on peak bed shear stresses it is denoted by $\Psi_{\tau*max}$ while $\Psi_{<\tau*>}$ is used when it is based on tidally averaged bed shear stresses.

At the grid locations where we determined the Shields number, we also determined the tidally averaged (U_0) and the M_2 tidal (U_{M2}) flow magnitudes, in a similar way as for the Shields number. Furthermore, we calculated the width-integrated and tidally averaged bedload and suspended load transport at the cross-sections shown in Figure 2.

3 Results

3.1 Evolution of control runs

Results of the two control simulations show that bed levels were initially not in morphodynamic equilibrium. The time-stack diagram of width-averaged depth as a function of space is shown in Figure 3. The morphology changed over time until an approximate equilibrium was reached, which took about 1200 years. There are two time-scales involved. First, there are deposition fronts from the upstream channel that migrate downstream. Second, there is a slower adaptation to the equilibrium condition. The results also show that true morphodynamic equilibrium, in the sense that bed levels are steady, was not achieved after 1200 years. However, bed level changes were small at the end of the simulation. The lowest discharge resulted in the smallest depth for the upstream channel, but the depth of the two downstream channels does not significantly affect the depth of the two downstream channels. This is because both control simulations were imposed by the same tidal forcing and the morphology of the downstream channels is mainly controlled by the tides ~~depend on the discharge~~. Typical depths are around 8 - 10 m for the downstream channels, and 10 – 12 m for the upstream one.

3.2 Geometry difference case

When simulations started with unequal channel depth, a similar evolution as the control simulations occurred. The morphological evolution was characterized by three typical time scales. First, there was erosion near the bifurcation, mainly because of the decrease in the cross-sectional area directly seaward of the bifurcation. Second, this erosion was followed by deposition fronts that migrated downstream during the simulation. This deposition front can be identified by a rapid decrease of the depth in the downstream channels at the beginning or halfway the simulation (Figure 4). It is similar to the evolution of

Control_Q2800 and Control_Q1596, but this depositional front was not necessarily similar in the two downstream channels because of the imposed differences in the initial bed level. Furthermore, in the lowest discharge simulations (Q=500 m^3s^{-1}) it takes much longer for the deposition front to reach downstream boundary and therefore it takes much longer before the system is in the steady state. Third, after the initial adaptation phase, the morphology of the channels started to change gradually. Some simulations took 2400 years (Q=500 m^3s^{-1}) until the morphological changes near the junction were small. Furthermore, the results show that at the end of the simulation the depth of the shallow branch depends on the discharge (Figure 4). The higher the discharge, the shallower the branch is. For the deepest branch it is the other way around. The deepest branch is shallowest for the lowest discharge.

The simulations that were based on perturbed equilibrium depth (Depth2) had a different morphological evolution and final equilibrium than the ones that started with 7.5 m depth difference (results not shown). The Depth2 simulation did not show the fast, initial depth response, but was mainly characterized by a slow adaptation to a new equilibrium because the system was still close to equilibrium at the start of the simulation. It took relatively long to achieve the new equilibrium and total simulation time was 2400 years in this case. Interestingly, although the external forcing for the Depth1 and Depth2 simulation were the same, the final equilibria were different. Because the depth in the channels influences the tidal dynamics (by for example the relative importance of friction and by difference in tidal propagation speed due to the different initial depths~~friction~~), the tide-induced flows were different at the junction and stayed different during the entire simulation. Hence, the equilibrium not only depends on external forcing but also on initial conditions. The initial and final morphology near the bifurcation for all Depth1 and Depth2 simulations can be seen in Appendix A.

The simulations with Length difference show that the shortest branch developed to be the deepest, while the longest became very shallow (Figure 5). The longest branch becomes so shallow that it becomes morphologically inactive. This occurred for both the highest and for the medium discharge scenario and is also independent of the initial conditions (starting with equilibrium bathymetry and shortened channel, or with 15 m deep channels). Meanwhile, the shortest channel was deepest for the highest discharge condition. The final morphology near the bifurcation for the simulations in Length difference scenario is provided in Appendix A.

3.3 Tide difference case

Asymmetric forcing of tides resulted in asymmetric morphological evolution. Because the system started out of equilibrium, the morphological evolution is again characterized by a quick adaptation followed by a slow evolution to the equilibrium. When forced by different tidal amplitude, the downstream branch with the smallest downstream tidal forcing evolved into the shallowest branch (Figure 6). Interestingly, when tidal amplitude in Branch 1 was decreased from 0.75 m to 0.5 m or even 0.25 m the bifurcation evolved into a less asymmetric system. Furthermore, when the two downstream channels were forced by equal amplitudes, but with different phase, this also resulted in the development of an asymmetric morphology of the

bifurcation (Figure 7). In general, the channel with delayed tides developed smallest channel depth while the channel with earlier tides developed deeper channels. Interestingly, the deposition front in the shallowest branch became stagnant for the largest imposed phase differences, suggesting that the flow magnitude was below the threshold for erosion (static equilibrium). However, the depth around the bifurcation did not become zero and still evolved. The larger the difference in tidal phase at the two downstream boundaries the shallower the delayed branch became, while the other branch was deeper. The final morphology near the bifurcation for all simulations of this case is provided in Appendix A.

4 Discussion

4.1 Relation between tides and the morphological evolution of bifurcations

The results suggest that tides cause less asymmetric bifurcations. To quantify how tides affect the morphology, the results from all scenarios were correlated. Figure 8 shows a scatter plot and linear fit between the final Ψ_h (dimensionless depth asymmetry) and Ψ_{τ^*} (dimensionless Shields asymmetry) for all model simulations. As can be seen, Ψ_h is linearly correlated with $\Psi_{<\tau^*>}$ and Ψ_{τ^*max}. Hence, the degree of asymmetry in the morphology is directly related to the degree of asymmetry in the sediment transport capacity. From comparison of $\Psi_{<\tau^*>}$ and Ψ_{τ^*max} against Ψ_h, Ψ_{τ^*max} shows the strongest relation and therefore the maximum mobility, which occurred during the peak ebb flow in our simulations, is the most representative to determine the morphological asymmetry of the downstream channels.

According to Eq. (3), in a system with uniform sediment properties and water density, the sediment mobility in the downstream channels only depends on the total bed shear stress τ_b. Because in the downstream channels the flows are mainly in along-channel direction, the instantaneous flow velocity to calculate the total bed shear stress τ_b in Eq. (4) ~~magnitude~~ can be represented~~expressed~~ by the ~~$\tau_b = \frac{\rho g u^2}{C^2}$, in which C is the Chézy coefficient and u is instantaneous~~ along-channel flow velocity. Based on a harmonic analysis, it became clear that the mean flow (U_0) and M_2 component (U_{M2}) were the main tidal constituents and higher harmonics like M_4 were relatively small. Therefore, the maximum sediment mobility scales very well with the square of summation of U_{M2} and U_0 ($\tau_{*max} \sim (U_{M2} + U_0)^2$).– The sediment mobility and flow conditions near the bifurcation for all simulations is provided in Table A1 in Appendix A.

The relatively strong river discharge in the simulations performed causes the ratios of U_0 and U_{M2} in the upstream channel cross section near the junction to be in the range between 0.2 ms^{-1} and values slightly larger than 1 ms^{-1} (see Figure a in Appendix A). This similar importance between those components indicates that our model is a mixed river- tide-influenced system. For most simulations, U_0, dominated by the river flow, in the two downstream branches was more asymmetric than U_{M2} (see Figure b Appendix A). In river-dominated systems, bifurcations with higher flow division asymmetry will also develop a more asymmetric morphology (Kleinhans et al., 2008). Interestingly, the tidal flows oppose the asymmetry induced

by U_0. U_{M2} becomes less asymmetric with the increase of tidal influence, shown by the decreasing trend in Ψ_{UM2} for increasing sum of U_{M2} ($\sum U_{M2}$) in the two downstream channels (Figure 9a), in which the summed U_{M2} was measured from the width-averaged U_{M2} at cross section in the downstream channels shown in Figure 2. This explains why the increased tidal influence, indicated by larger sum of U_{M2} in Figure 9a and Figure 9b, causes less asymmetric bifurcations. Due to tides, the sediment mobility in both channels is closer to each other than without tides (Figure 9b). A more tide influenced condition is not only achieved by decreasing river discharge, but also by inducing an asymmetry in the tidal forcing in the downstream channels. For either increased difference in amplitude or phase, the sum of U_{M2} in both downstream channels also increased and became similar in magnitude. The scatter in the results shown in Figure 9 is caused by the different imposed asymmetries for different scenarios. The asymmetry is not only controlled by external forcing, but also determined by internal dynamics when the depth of the branches develop, and because we have different types of initial asymmetries (forcing, depth, length), there is quite some scatter in Figure 9. Still, we found that all simulations have a similar behaviour, i.e. more tidal influence drives a less morphological asymmetry between downstream channels.

There are two ~~reasons~~ processes that drive a less asymmetric tidal flow in the more tide influenced condition. First, the propagation of tides from the dominant downstream channel to the other downstream channel balances the tidal flow in the two downstream channels. This process mainly rules in tide difference case. Tidal forcing asymmetry between downstream channels drives tidal propagation from one downstream channel to the other and results in phase lags of tidal flow inducing strong cross-channel flow at the junction (similarly as discussed in Buschman et al., 2013). This can be seen by a larger cross-channel flow in the upstream channel near the bifurcations for larger asymmetry between the prescribed tides in Figure 10. This cross-channel flow is dominated by the tides (V_{M2}) while its mean flow value (V_0) was close to zero. Strong cross-channel flows caused erosion at the bifurcation, resulting in a trench-like scour connecting the downstream channels. This scour can be found in the amplitude phase difference scenario and the most pronounced in the simulation Amp_0.25 (see Figure A2c-f in Appendix A). Although a bar developed in the upstream channel on the side of the downstream channel imposed with lower tidal amplitude, the cross-channel flows deepened the bed at bifurcation and maintained the connection between both downstream channels and the upstream channel. The development of the trench-like scour at the bifurcations is also observed in the Berau River Delta (Buschman et al., 2013) and Mahakam Delta (Sassi et al., 2011). This deepening at the bifurcation can be also affected by the angle of the bifurcation, something we did not study here. Second, with equal tides imposed in the two downstream channels for depth and length difference scenario, the larger river discharge in the dominant downstream channel dampens the tides in this channel while the shallowing bed level in the other downstream channel increase the tidal flow in this channel. As a result, this combining effect induces a less asymmetric tidal flow in the downstream channels.

4.2 Role of bedload versus suspended load

In the theory of Bolla Pittaluga et al. (2003) and Bolla Pittaluga et al. (2015) the lateral bed slope causes additional sediment transport into the dominant channel, thereby having a stabilizing effect on the bifurcation. Here, we used the van Rijn (1993)

sediment transport formulations in which bed slope only affects the bedload transport and not the suspended load transport~~.~~. Based on this, we expected that bedload transport will be divided less asymmetrically than suspended load transport. To check this hypothesis, the tidally averaged and width-integrated sediment transport at the cross-sections, shown in Figure 2, were calculated. We calculated an asymmetry index similar as we did for the Shields number and depth. The results of the scatter plot of suspended load asymmetry versus bedload asymmetry index clearly show that suspended load tends to be divided more asymmetric at the bifurcation (Figure 11a). Only when the system is fully symmetric or asymmetric there is no difference in asymmetry of bedload and suspended load transport because the downstream channels receive an equal amount of sediment when the downstream channels are symmetric, while only one downstream channel receives all sediment when an avulsion occurs (both bedload and suspended load asymmetry are 1). ~~Note that this asymmetry trend could be different for different sediment grain size. A finer sediment defined would result in a large sediment mobility which weaken the effect of lateral bed slope to oppose the asymmetric division of bedload transport. Thus the asymmetry of bedload and suspended load would tend to be more similar.~~ Furthermore, from a scatter plot of depth asymmetry (ψ_h) versus the ratio of bedload transport over suspended load transport in the upstream channel, it becomes clear that systems that have more asymmetric bed levels have a smaller contribution of bedload transport to the total transport, and vice versa (Figure 11b). However, there is also some considerable scatter due to the sensitivity to the initially imposed asymmetry. Lastly, a scatter plot of the ratio of mean flow and M_2 flow magnitude versus ratio of bedload and suspended load transport in the upstream channel (Figure 11c) suggest that when river flow is relatively important, the system is suspended load dominated, while for more tide-dominated conditions bedload plays a more important role. This further explains why the more tide-dominated conditions result in less asymmetric morphology.

4.3 Sensitivity to sediment grain size and lateral bedslope effect

Defining a different sediment grain size would change the sediment mobility and drive a different ratio of suspended load and bedload transport. These would affect the sediment transport division and therefore the morphological development in the downstream channels. When using finer sediment this results in a more asymmetric development of the downstream channels, as is shown in Figure 12. The finer sand induces a larger contribution of suspended load transport to total sediment transport and therefore counteracts the stabilizing effect by the transverse bedslope effect on the bedload. As a result, the depth asymmetry between downstream channels increases. Similarly, a coarser sediment results in smaller depth asymmetry between the downstream channels.

The importance of lateral bedslope effect to oppose the asymmetrical morphological development between downstream channels causes the model results to be sensitive to the parameter α_{bn}. Using physical scale models, previous studies have suggested that α_{bn} value should take values between 0.2-1.5 (Baar et al., 2018; Ikeda, 1982; Schuurman et al., 2013; Talmon et al., 1995). However, Delft3D shows unrealistic morphological development when small values of α_{bn} are used, as shown in Figure 13. Simulation Depth1_Q2800 with small α_{bn} (α_{bn}=1) showed the development of an elongated bar upstream on the side

of shallow downstream channel and a large incision occurred on the other side. This unrealistic behaviour has also been evaluated by Baar et al. (2019). The use of small value of α_{bn} causes the morphological development to be dependent on the grid size (Baar et al., 2019). Several studies have used much higher value to overcome this issue (e.g. Dissanayake et al., 2009; van der Wegen and Roelvink, 2012; Van Der Wegen and Roelvink, 2008). Using our model set-up, the model results started to be insensitive to the value of α_{bn} when α_{bn} is 10. Using this value the lateral slope developing upstream of the bifurcation is less than threefold of upstream channel width as also suggested by Bolla Pittaluga et al. (2003) and Kleinhans et al. (2008) for river dominated bifurcations.

4.4 Implications of results

From the findings presented in this paper, we can predict how tides will influence the morphological evolution of deltas. In the seaward part of tide-influenced deltas, especially those with seaward widening channels, river flow tends to be small relative to ~~and~~ the tidal flows. In these regions we only expect asymmetry in morphology when the branches are unequally forced by tides. The tides tend to keep all the branches open and have similar depths. In the upstream part of deltas, river flows tend to be larger which can result in large morphological asymmetries. However, the different possible pathways of the tide along the channel networks can generate differences in tidal amplitude and tidal phase between branches, inducing relatively strong tidal currents at the junction. This prevents the closure of one downstream channel and erodes the bed at the junction because of the strong cross-channel flows.

Morphological development of bifurcations occurs on a long time scale and several ~~effects~~ external causes and internal processes neglected here can affect bifurcation stability~~have been neglected~~ (also see review in Kleinhans et al., 2013), such as of sea level rise (Jerolmack, 2009; Van Der Wegen, 2013), changes in upstream discharge or sediment supply (Syvitski and Milliman, 2007), channel bank erosion or growth (Miori et al., 2006) and delta front development that could change the length of a branch (Salter et al., 2017). However, we have provided a basic explanation on how tides can stabilize the morphology of deltas.

5 Conclusions

In this manuscript, the effect of tides on the morphological development of bifurcations was investigated using a numerical modelling approach in Delft3D. An idealized bifurcation was built by splitting an upstream channel into two downstream branches. The idealized bifurcations were forced by river discharge from upstream and tides from downstream. To identify the effect of tides, two cases were studied, namely geometry difference (length and depth of channels) and tide difference (difference in prescribed tides at the two downstream channels).

The results show that increased tidal influence compared to river influence, results in a less asymmetric morphology of the bifurcation. This increased tidal influence can either be achieved by smaller river discharge or by asymmetric tides from downstream. The main mechanism is that tidal flows tend to be less asymmetric in the two downstream channels than tidally averaged flows. This causes the peak Shields number in the branches to be closer to each other with increasing influence of tides. Furthermore, we have shown that bedload transport tends to be divided less asymmetrically than suspended load due to the influence of lateral bed slopes, which tends to ~~on~~ stabilize the system. In our simulations, bifurcations with increased tidal influence had a relatively high ratio of bedload over suspended load transport and therefore developed a less asymmetric morphology than in river-dominated systems. Our results can explain why tides tend to stabilize the bifurcations in deltas.

Code availability

The model setup for all Delft3D simulations is provided in the Supplement. The results presented were simulated using Delft3D software package (Delft3D-flow version 4.01.00.rc.04).

Author contribution

API, MvdV, and MGK designed the study. API conducted the numerical modelling, performed the output analysis and interpretation, and wrote the manuscript with major input from MvdV and MGK. MvdV conducted part of the output analysis and edited the paper.

Competing interests

The authors declare that they have no conflict of interest.

Acknowledgments

This research is funded by Indonesia Endowment Fund for Education (LPDP) grant to A.P. Iwantoro.

References

Alebregtse, N. C. and de Swart, H. E.: Effect of river discharge and geometry on tides and net water transport in an estuarine network, an idealized model applied to the Yangtze Estuary, Cont. Shelf Res., 123, 29–49, doi:10.1016/j.csr.2016.03.028, 2016.

Baar, A. W., de Smit, J., Uijttewaal, W. S. J. and Kleinhans, M. G.: Sediment Transport of Fine Sand to Fine Gravel on Transverse Bed Slopes in Rotating Annular Flume Experiments, Water Resour. Res., 54(1), 19–45,

doi:10.1002/2017WR020604, 2018.

Baar, A. W., Boechat Albernaz, M., van Dijk, W. M. and Kleinhans, M. G.: Critical dependence of morphodynamic models of fluvial and tidal systems on empirical downslope sediment transport, Nat. Commun., 10(1), doi:10.1038/s41467-019-12753-x, 2019.

Bagnold, R. A.: An Approach to the Sediment Transport Problem from General Physics., USGS Prof. Pap., 42, doi:10.1017/S0016756800049074, 1966.

Bertoldi, W. and Tubino, M.: River bifurcations: Experimental observations on equilibrium configurations, Water Resour. Res., 43(10), doi:10.1029/2007WR005907, 2007.

Blondeaux, P. and Seminara, G.: A unified bar–bend theory of river meanders, J. Fluid Mech., 157(HY11), 449–470, doi:10.1017/S0022112085002440, 1985.

Bolla Pittaluga, M., Repetto, R. and Tubino, M.: Channel bifurcation in braided rivers: Equilibrium configurations and stability, Water Resour. Res., 39(3), 1–13, doi:10.1029/2003WR002754, 2003.

Bolla Pittaluga, M., Coco, G. and Kleinhans, M. G.: A unified framework for stability of channel bifurcations in gravel and sand fluvial systems, Geophys. Res. Lett., 42(18), 7521–7536, doi:10.1002/2015GL065175, 2015.

Buschman, F. a., van der Vegt, M., Hoitink, a. J. F. and Hoekstra, P.: Water and suspended sediment division at a stratified tidal junction, J. Geophys. Res. Ocean., 118(3), 1459–1472, doi:10.1002/jgrc.20124, 2013.

Buschman, F. A., Hoitink, A. J. F., van der Vegt, M. and Hoekstra, P.: Subtidal flow division at a shallow tidal junction, Water Resour. Res., 46(12), W12515, doi:10.1029/2010WR009266, 2010.

Chen Ji-Yu, Yun Cai-xing, X. H.: The model of development of the Changjiang estuary during the last 2000 years, in Proceedings of the Sixth Biennial International Estuarine Research Conference, pp. 655–666., 1982.

Daniel, G., Brad, H., Miodrag, S., Forrest, H., Hasan, P. and Nolan, R.: Application of 3D Mobile Bed, Hydrodynamic Model, J. Hydraul. Eng., 125(7), 737–749, doi:10.1061/(ASCE)0733-9429(1999)125:7(737), 1999.

Dissanayake, D. M. P. K., Roelvink, J. a. and van der Wegen, M.: Modelled channel patterns in a schematized tidal inlet, Coast. Eng., 56(11–12), 1069–1083, doi:10.1016/j.coastaleng.2009.08.008, 2009.

Edmonds, D. A. and Slingerland, R. L.: Mechanics of river mouth bar formation: Implications for the morphodynamics of delta distributary networks, J. Geophys. Res. Earth Surf., doi:10.1029/2006JF000574, 2007.

Frings, R. M. and Kleinhans, M. G.: Complex variations in sediment transport at three large river bifurcations during discharge waves in the river Rhine, Sedimentology, 55, 1145–1171, doi:10.1111/j.1365-3091.2007.00940.x, 2008.

Galloway, W. E.: Process framework for describing the morphologic and stratigraphic evolution of deltaic systems, in Deltas, Models for Exploration., 1975.

Geleynse, N., Storms, J. E. A., Walstra, D. J. R., Jagers, H. R. A., Wang, Z. B. and Stive, M. J. F.: Controls on river delta formation; insights from numerical modelling, Earth Planet. Sci. Lett., doi:10.1016/j.epsl.2010.12.013, 2011.

Hoitink, A. J. F., Wang, Z. B., Vermeulen, B., Huismans, Y. and Kästner, K.: Tidal controls on river delta morphology, Nat. Geosci., 10(9), 637–645, doi:10.1038/ngeo3000, 2017.

Ikeda, S.: Incipient Motion of Sand Particles on Side Slopes, J. Hydraul. Div., 108(1), 95–114, 1982.

Jerolmack, D. J.: Conceptual framework for assessing the response of delta channel networks to Holocene sea level rise, Quat. Sci. Rev., doi:10.1016/j.quascirev.2009.02.015, 2009.

Kästner, K., Hoitink, A. J. F., Vermeulen, B., Geertsema, T. J. and Ningsih, N. S.: Distributary channels in the fluvial to tidal transition zone, J. Geophys. Res. Earth Surf., 122(3), 696–710, doi:10.1002/2016JF004075, 2017.

Kleinhans, M. G. and van den Berg, J. H.: River channel and bar patterns explained and predicted by an empirical and a physics-based method, Earth Surf. Process. Landforms, 36(6), 721–738, doi:10.1002/esp.2090, 2011.

Kleinhans, M. G., Jagers, H. R. a, Mosselman, E. and Sloff, C. J.: Bifurcation dynamics and avulsion duration in meandering rivers by one-dimensional and three-dimensional models, Water Resour. Res., 44(8), 1–31, doi:10.1029/2007WR005912, 2008.

Kleinhans, M. G., Ferguson, R. I., Lane, S. N. and Hardy, R. J.: Splitting rivers at their seams: Bifurcations and avulsion, Earth Surf. Process. Landforms, 38(1), 47–61, doi:10.1002/esp.3268, 2013.

Lane, S. N., Bradbrook, K. F., Richards, K. S., Biron, P. A. and Roy, A. G.: The application of computational fluid dynamics to natural river channels: three-dimensional versus two-dimensional approaches, Geomorphology, 29(1), 1–20, doi:https://doi.org/10.1016/S0169-555X(99)00003-3, 1999.

Leonardi, N., Canestrelli, A., Sun, T. and Fagherazzi, S.: Effect of tides on mouth bar morphology and hydrodynamics, J. Geophys. Res. Ocean., doi:10.1002/jgrc.20302, 2013.

Lesser, G. R., Roelvink, J. a., van Kester, J. a T. M. and Stelling, G. S.: Development and validation of a three-dimensional morphological model, Coast. Eng., 51(8–9), 883–915, doi:10.1016/j.coastaleng.2004.07.014, 2004.

Miori, S., Repetto, R. and Tubino, M.: A one-dimensional model of bifurcations in gravel bed channels with erodible banks, Water Resour. Res., 42(11), doi:10.1029/2006WR004863, 2006.

Nnafie, A., Van Oyen, T., De Maerschalck, B., van der Vegt, M. and van der Wegen, M.: Estuarine Channel Evolution in Response to Closure of Secondary Basins: An Observational and Morphodynamic Modeling Study of the Western Scheldt Estuary, J. Geophys. Res. Earth Surf., doi:10.1002/2017JF004364, 2018.

Redolfi, M., Zolezzi, G. and Tubino, M.: Free instability of channel bifurcations and morphodynamic influence, J. Fluid Mech., 799, 476–504, doi:10.1017/jfm.2016.389, 2016.

Redolfi, M., Zolezzi, G. and Tubino, M.: Free and forced morphodynamics of river bifurcations, Earth Surf. Process. Landforms, 44(4), 973–987, doi:10.1002/esp.4561, 2019.

van Rijn, L.: Principles of Sediment Transport in Rivers, Estuaries and Coastal Seas, Princ. Sediment Transp. Rivers , Estuaries Coast. Seas, 11–31, doi:10.1002/9781444308785, 1993.

Roelvink, J. a.: Coastal morphodynamic evolution techniques, Coast. Eng., 53(2–3), 277–287, doi:10.1016/j.coastaleng.2005.10.015, 2006.

Rossi, V. M., Kim, W., López, J. L., Edmonds, D., Geleynse, N., Olariu, C., Steel, R. J., Hiatt, M. and Passalacqua, P.: Impact of tidal currents on delta-channel deepening, stratigraphic architecture, and sediment bypass beyond the shoreline, Geology,

doi:10.1130/G38334.1, 2016.

Salter, G., Paola, C. and Voller, V. R.: Control of Delta Avulsion by Downstream Sediment Sinks, J. Geophys. Res. Earth Surf., 123(1), 142–166, doi:10.1002/2017JF004350, 2017.

Sassi, M. G., Hoitink, a. J. F., De Brye, B., Vermeulen, B. and Deleersnijder, E.: Tidal impact on the division of river discharge over distributary channels in the Mahakam Delta, Ocean Dyn., 61(12), 2211–2228, doi:10.1007/s10236-011-0473-9, 2011.

Schuurman, F., Marra, W. A. and Kleinhans, M. G.: Physics-based modeling of large braided sand-bed rivers: Bar pattern formation, dynamics, and sensitivity, J. Geophys. Res. Earth Surf., 118(4), 2509–2527, doi:10.1002/2013JF002896, 2013.

Shaw, J. B. and Mohrig, D.: The importance of erosion in distributary channel network growth, Wax Lake Delta, Louisiana, USA, Geology, doi:10.1130/G34751.1, 2014.

Stephens, J. D., Allison, M. A., Di Leonardo, D. R., Weathers, H. D., Ogston, A. S., McLachlan, R. L., Xing, F. and Meselhe, E. A.: Sand dynamics in the Mekong River channel and export to the coastal ocean, Cont. Shelf Res., 147, 38–50, doi:10.1016/j.csr.2017.08.004, 2017.

Struiksma, N., Olesen, K. W., Flokstra, C. and De Vriend, H. J.: Bed deformation in curved alluvial channels, J. Hydraul. Res., 23(1), 57–79, doi:10.1080/00221688509499377, 1985.

Syvitski, J. P. M. and Milliman, J. D.: Geology, geography, and humans battle for dominance over the delivery of fluvial sediment to the coastal ocean, J. Geol., doi:10.1086/509246, 2007.

Talmon, A. M., Struiksma, N. and Van Mierlo, M. C. L. M.: Laboratory measurements of the direction of sediment transport on transverse alluvial-bed slopes, J. Hydraul. Res., 33(4), 495–517, doi:10.1080/00221689509498657, 1995.

Wang, Z. B., De Vries, M., Fokkink, R. J. and Langerak, a.: Stability of river bifurcations in ID morphodynamic models, J. Hydraul. Res., 33(6), 739–750, doi:10.1080/00221689509498549, 1995.

van der Wegen, M. and Roelvink, J. A.: Reproduction of estuarine bathymetry by means of a process-based model: Western Scheldt case study, the Netherlands, Geomorphology, 179, 152–167, doi:10.1016/j.geomorph.2012.08.007, 2012.

van der Wegen, M., Wang, Z. B., Savenije, H. H. G. and Roelvink, J. A.: Long-term morphodynamic evoluation and energy dissipation in a coastal plain, tidal embayment, J. Geophys. Res. Earth Surf., 113(3), doi:10.1029/2007JF000898, 2008.

Van Der Wegen, M.: Numerical modeling of the impact of sea level rise on tidal basin morphodynamics, J. Geophys. Res. Earth Surf., doi:10.1002/jgrf.20034, 2013.

Van Der Wegen, M. and Roelvink, J. a.: Long-term morphodynamic evolution of a tidal embayment using a two-dimensional, process-based model, J. Geophys. Res. Ocean., 113(3), 1–23, doi:10.1029/2006JC003983, 2008.

Zhang, E. F., Savenije, H. H. G., Chen, S. L. and Mao, X. H.: An analytical solution for tidal propagation in the Yangtze Estuary, China, Hydrol. Earth Syst. Sci., 16(9), 3327–3339, doi:10.5194/hess-16-3327-2012, 2012.

Table 1: Summary of simulations undertaken in the present study and their boundary conditions (river discharge and tidal properties), and geometry differences between the downstream channels.

Scenario	Simulation name	Q (m^3s^{-1})	η_{M2} (m)		$\Delta\theta_{M2}$ (º)	ΔL (km)	Δh (m)
			Branch 1	Branch 2			
Control simulation	Control_Q2800	2800	1	1	0	0	0
	Control_Q1596	1596	1	1	0	0	0
Depth difference	Depth1_Q2800	2800	1	1	0	0	7.5
	Depth1_Q1596	1596	1	1	0	0	7.5
	Depth1_Q500	500	1	1	0	0	7.5
	Depth2_Q2800	2800	1	1	0	0	1
	Depth2_Q1596	1596	1	1	0	0	1
Length difference	Length_Q2800	2800	1	1	0	15	0
	Length_Q1596	1596	1	1	0	15	0
Amplitude difference	Amp_0.75	2800	0.75	1	0	0	0
	Amp_0.5		0.5	1	0	0	0
	Amp_0.25		0.25	1	0	0	0
Phase difference	Phase_10	2800	1	1	10	0	0
	Phase_22.5		1	1	22.5	0	0
	Phase_35		1	1	35	0	0

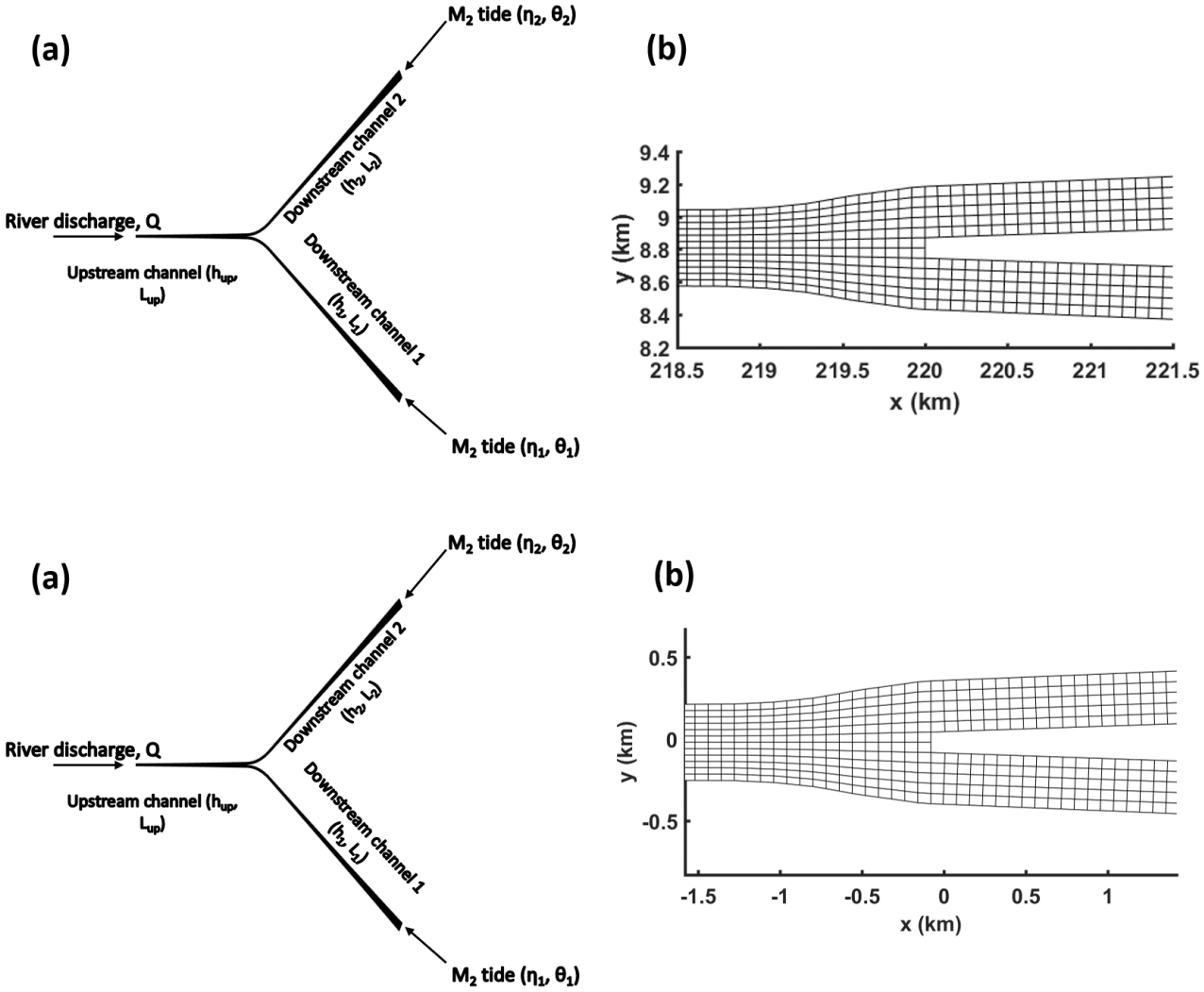

Figure 1: (a) Illustration of bifurcation model setup from the upstream channel forced by river discharge Q, to the downstream boundaries which are forced by tidal water levels. Here, h indicates the depth and L indicates the length of each channel. Meanwhile, Η and θ indicates amplitude and phase of tidal water levels at each downstream boundary. (b) Zoom of model grid near the junction, showing the additional widening near the junction and the disappearance of two grid cells downstream of the junction.

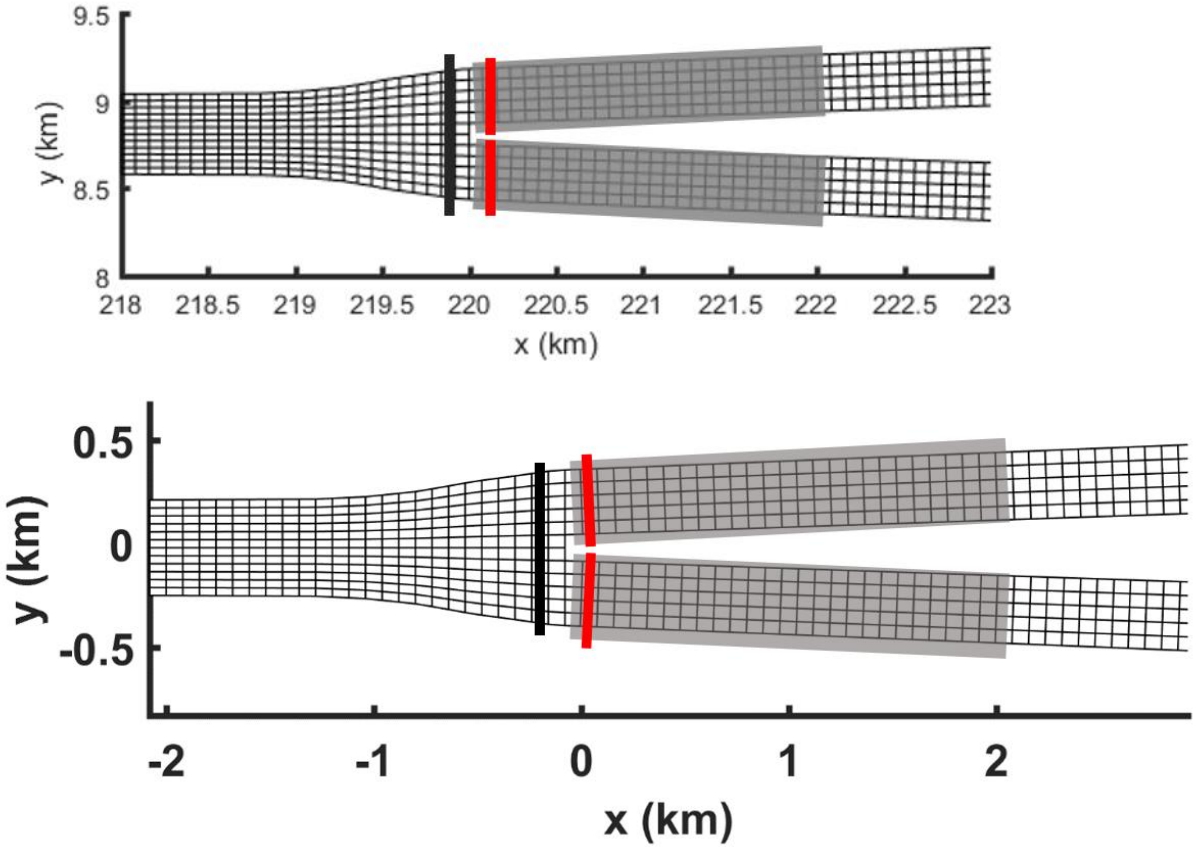

Figure 2: The grids in surrounding of the bifurcation overlaid by the areas where the bed level changes were evaluated (grey boxes), the grids where the asymmetry indices (red lines) and upstream channel flow (black line) were calculated.

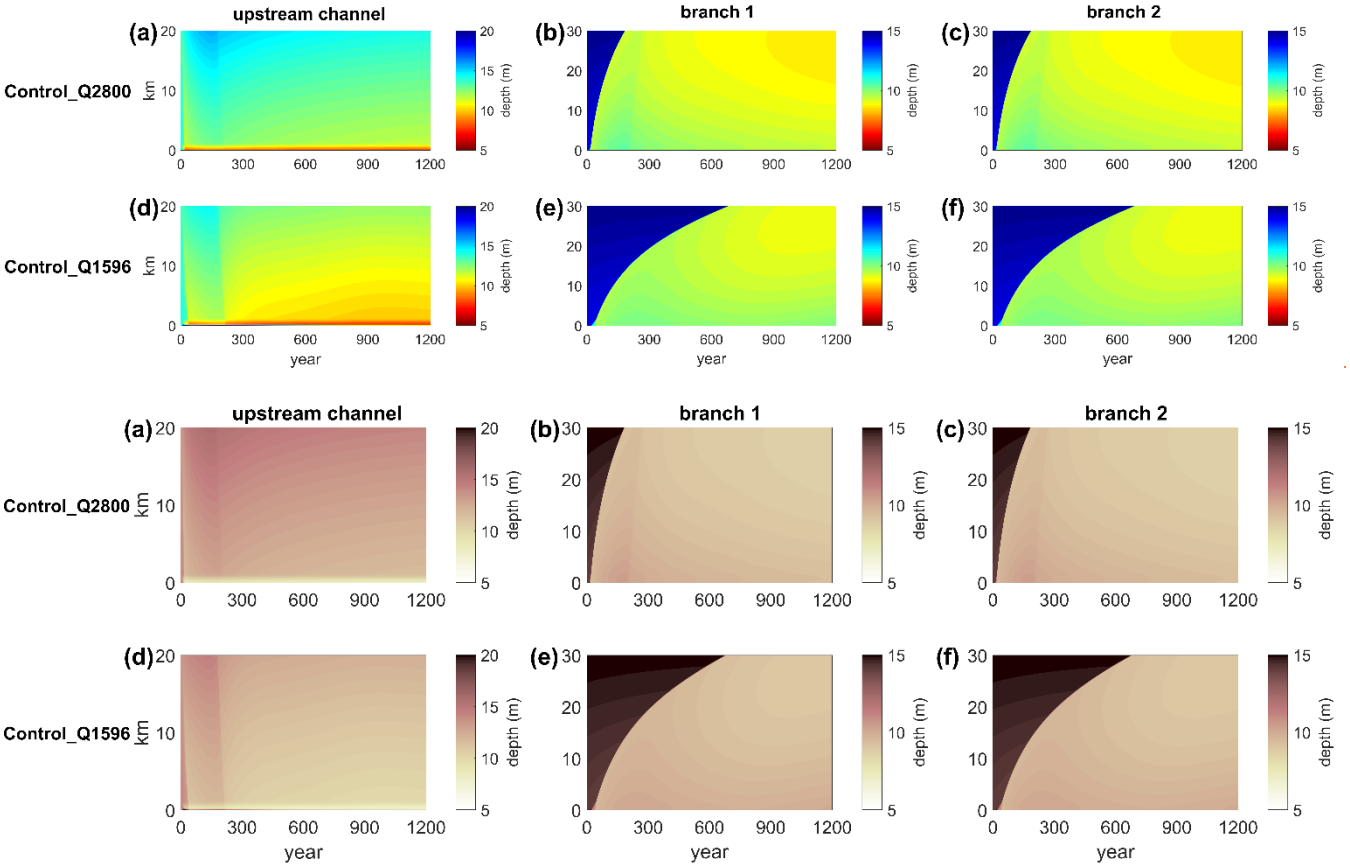

Figure 3: Time-stack diagram of width- and tide-averaged depth (colour) of the upstream channel (left panels; km 0 is junction, km 20 upstream) and downstream channels (middle and right panels; km 0 is junction, km 30 near sea) as a function of distance from the bifurcation (vertical axis) for the two control simulations. The top panels ((a), (b), and (c)) are the result from the high discharge simulation (Control_Q2800) while the bottom panels ((d), (e), and (f)) are for the low discharge simulation (Control_Q1596).

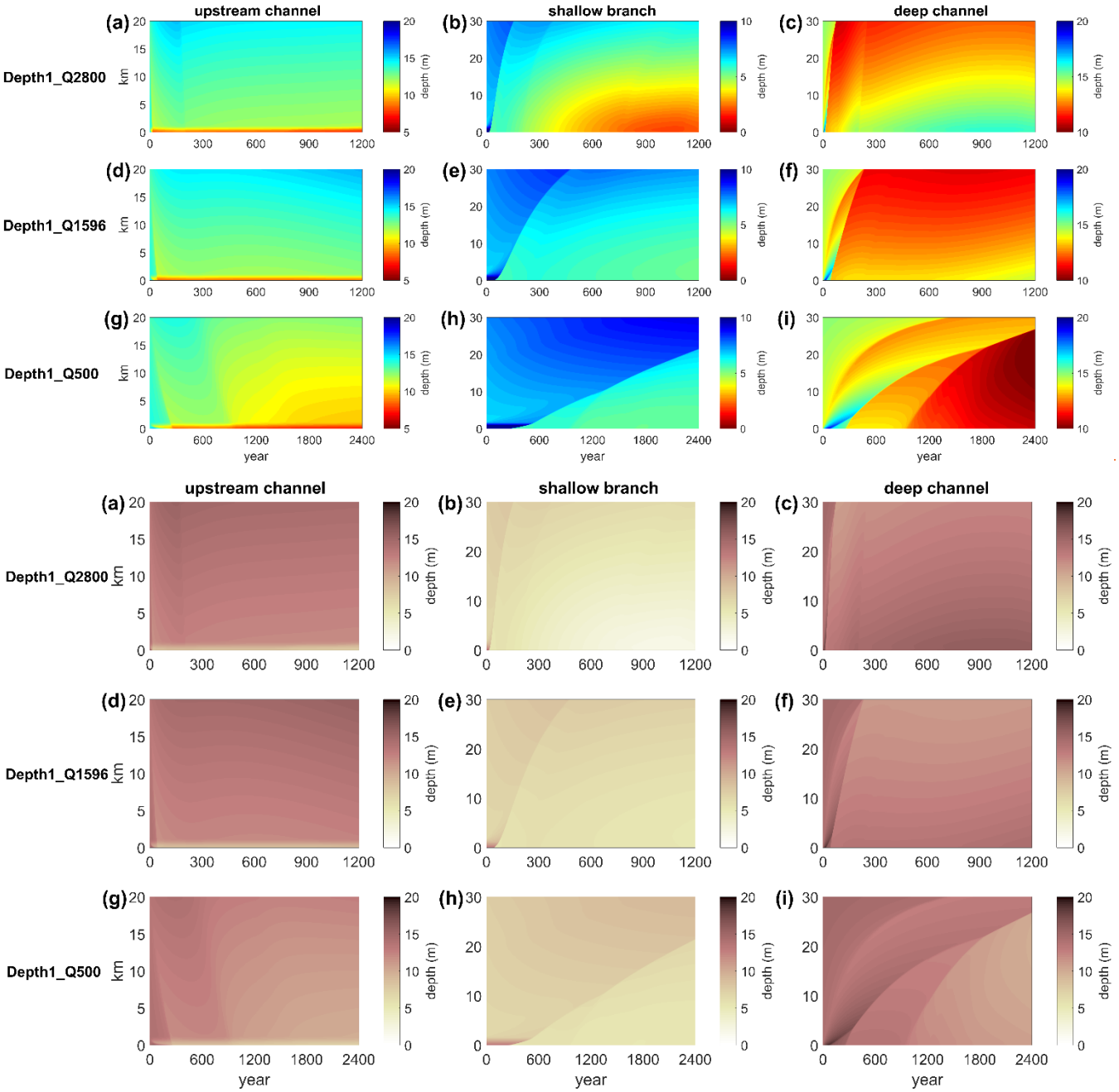

Figure 4: Same plot as Figure 3 but for simulations of Depth1. The panels from top to bottom show the results from different simulation (Depth1_Q2800, Depth1_Q1596, Depth1_Q500, respectively) while from left to right show the upstream channel, shallow branch, and deep branch, respectively. Different scale of colour bar for different channel is applied.

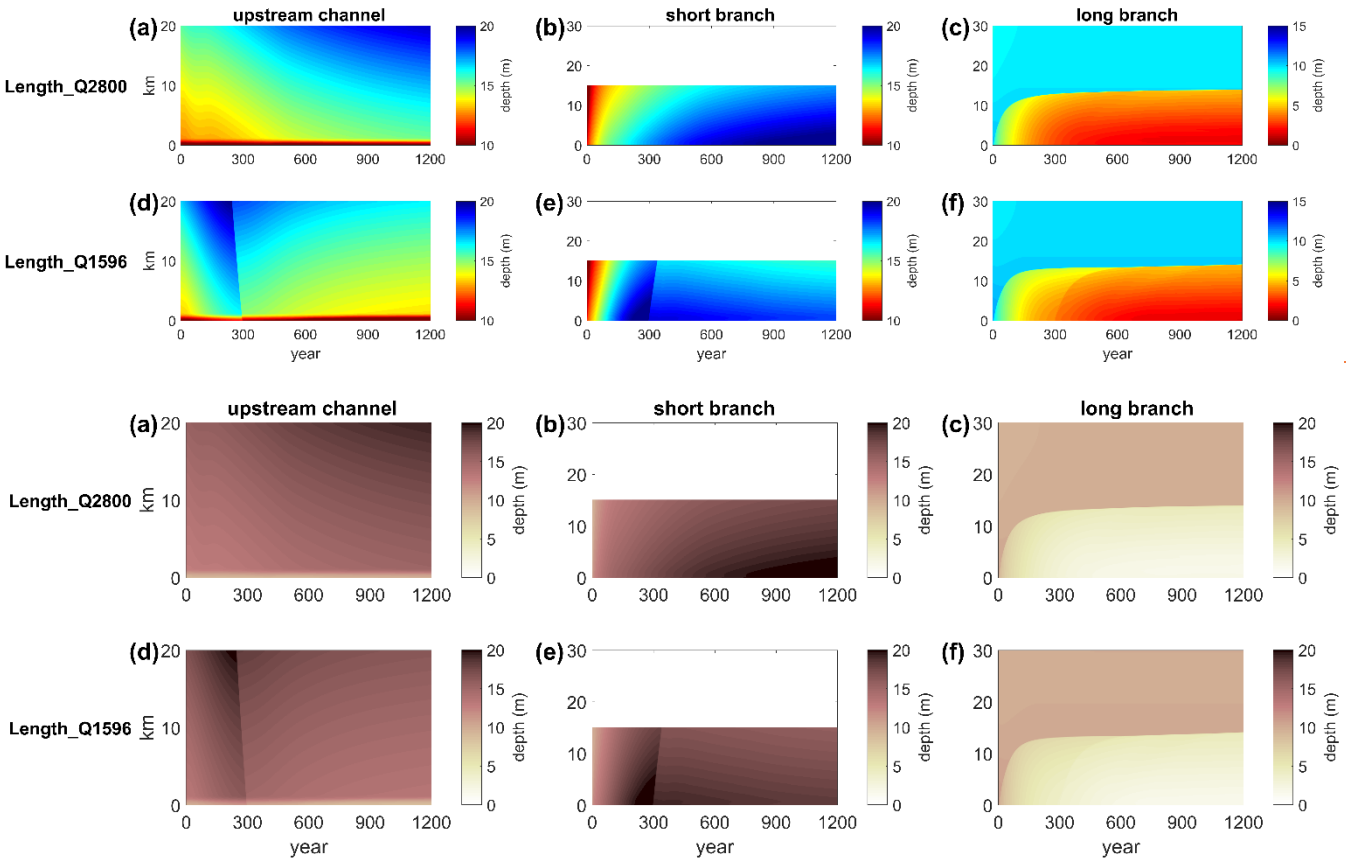

Figure 5: Time-stack diagram of width- and tide-averaged depth as a function of space for the simulations in Length difference scenario with the same order as Figure 4 but with short (panel (b) and (e)) and long (panel (c) and (f)) downstream branch.

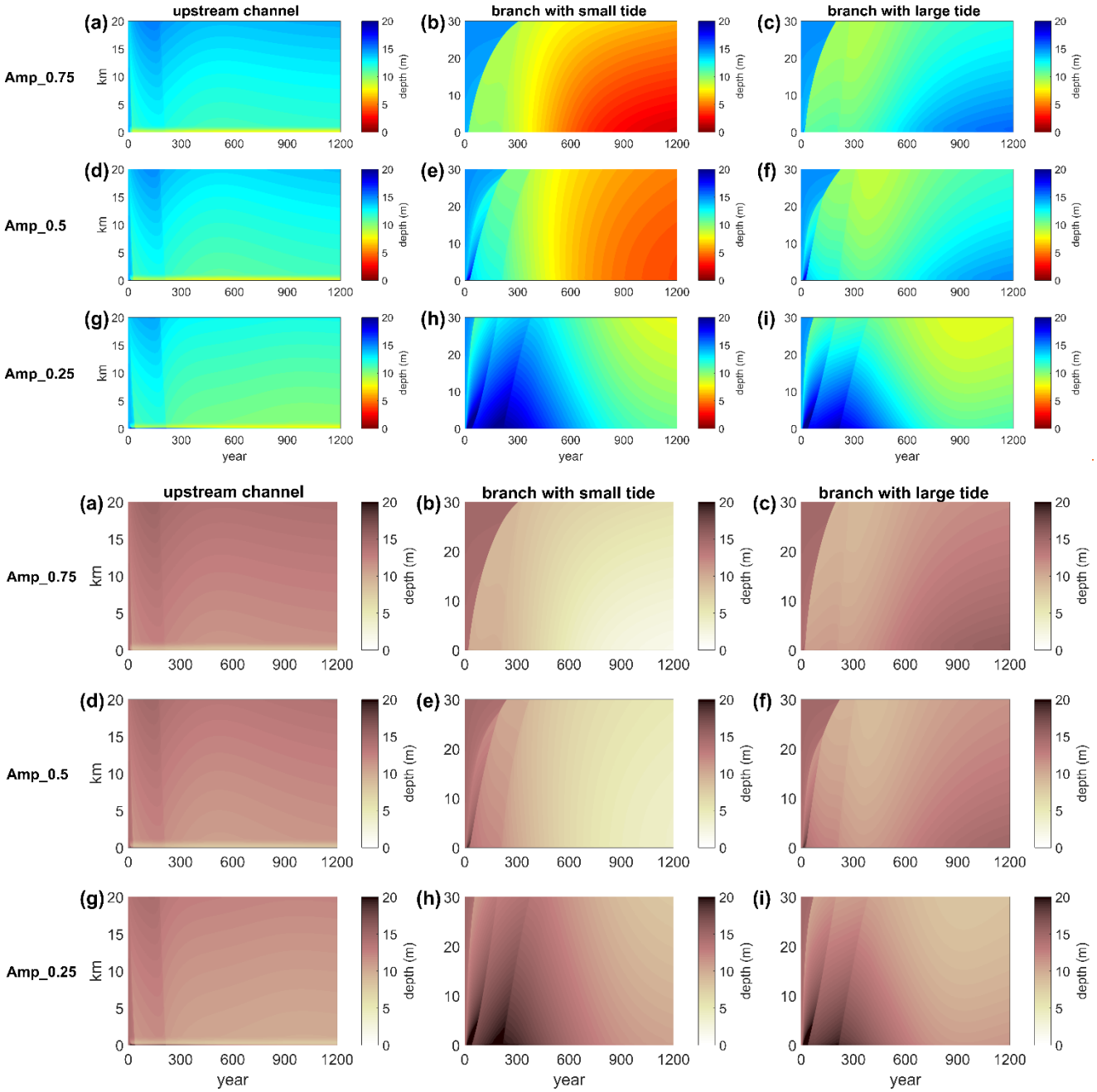

Figure 6: Time-stack diagram of width- and tide-averaged depth as a function of space for the Amplitude difference scenario.

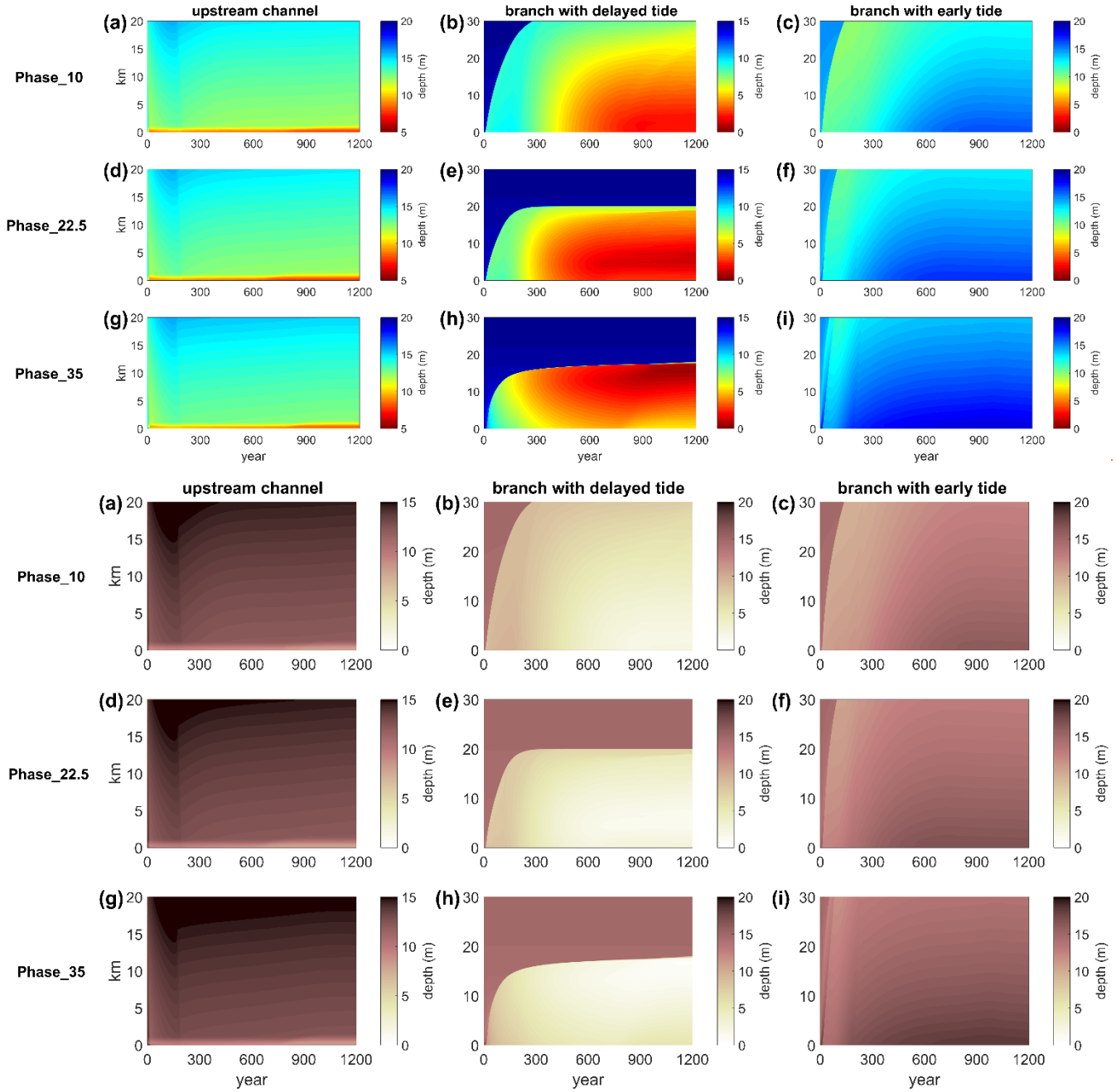

Figure 7: Time-stack diagram of width- and tide-averaged depth as a function of space for Phase difference scenario.

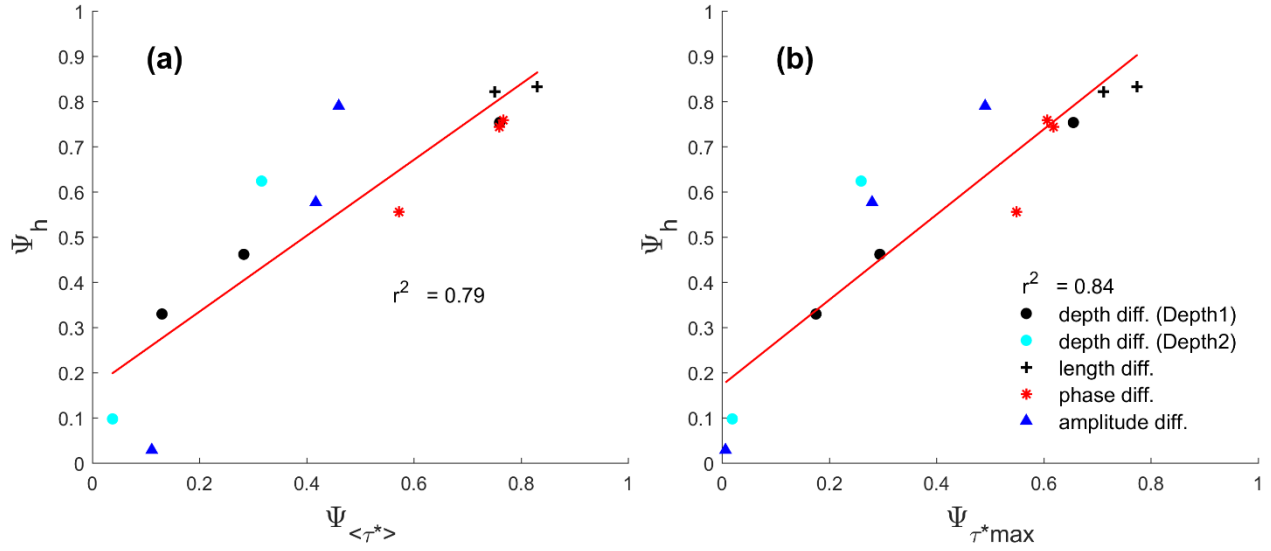

Figure 8: Relation between depth asymmetry number Ψ_h and: (a) the asymmetry in tidally averaged Shields number ($\Psi_{<\tau^*>}$), and (b) the asymmetry in peak Shields number (Ψ_{τ^*max}) at the equilibrium condition for all simulations from scenarios described in Table 1. Note that in panel a, two simulations of Phase difference scenario and a simulation of Depth1 scenario is slightly overlapping.

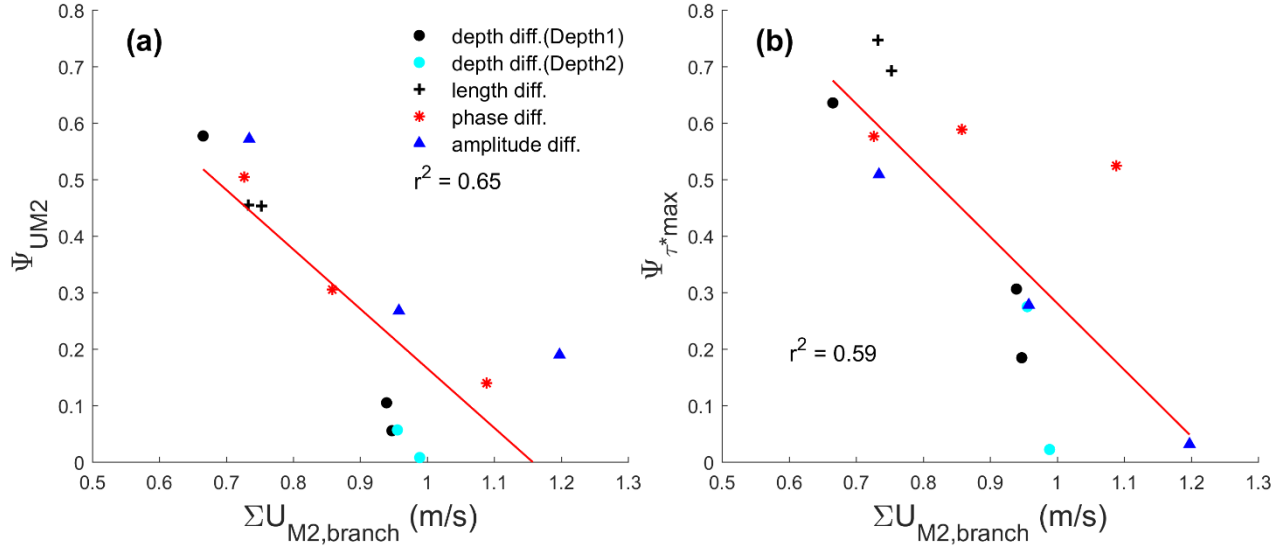

Figure 9: Comparison between: (a) tidal flow asymmetry and (b) Peak Shields number asymmetry in the two downstream branches against the total tidal flow magnitude from the two downstream channels.

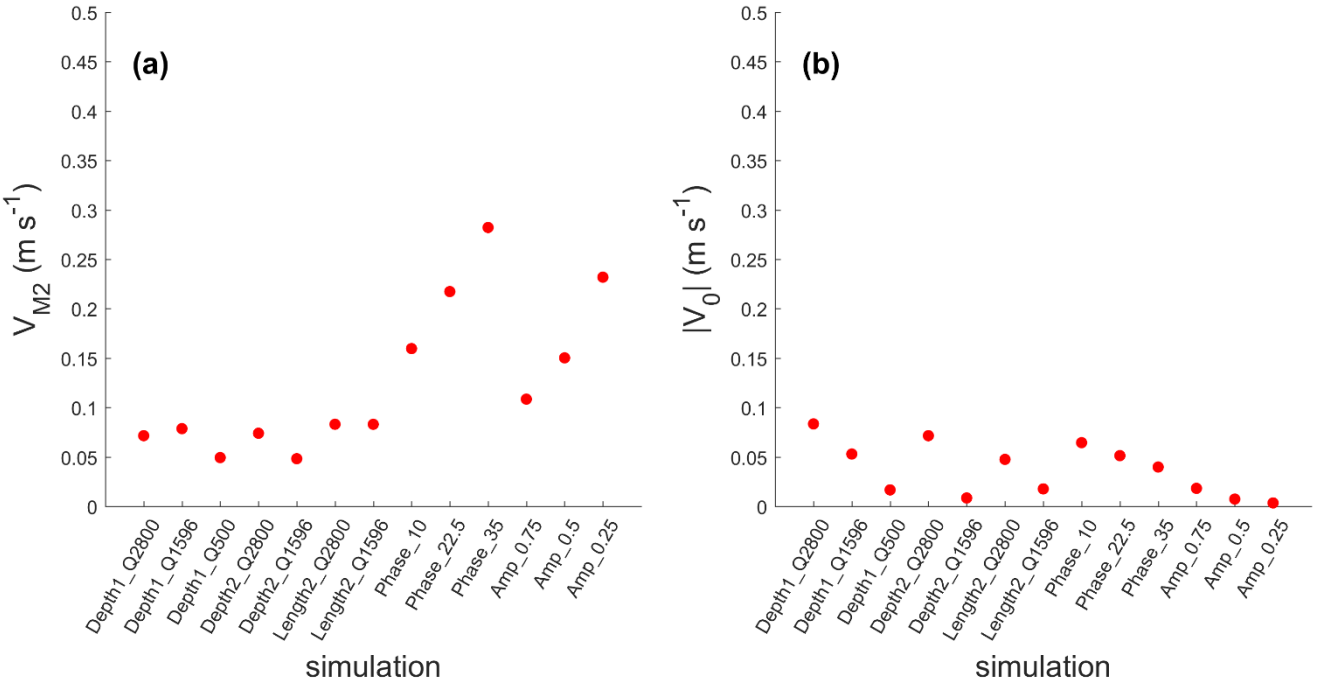

Figure 10: Cross channel flow of: (a) tidal current amplitude and (b) mean current at bifurcation in the upstream channel for all simulations.

590

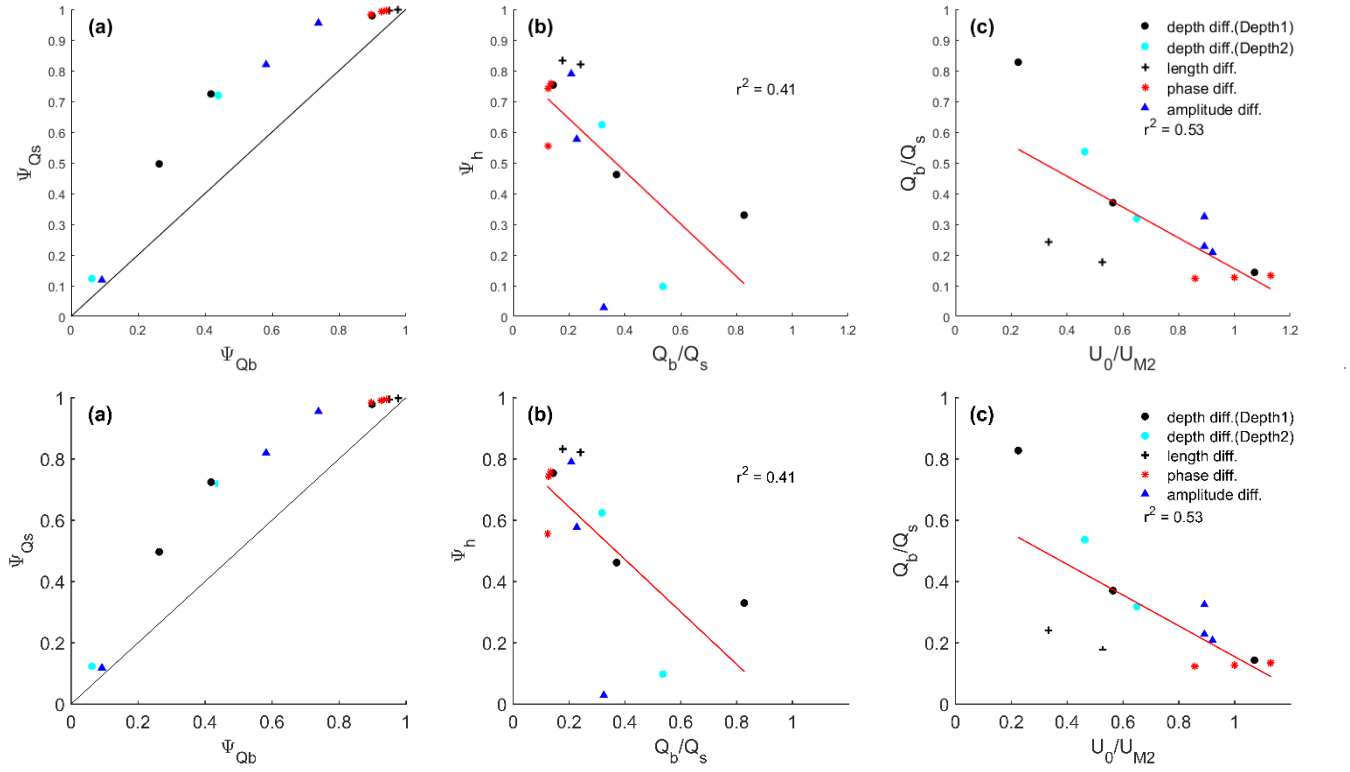

Figure 11: Comparison of: (a) Suspended load asymmetry ($\Psi_{susp\ load}$) against bedload asymmetry ($\Psi_{bedload}$) overlaid by the line of equality (black line), (b) Scatter plot of morphology asymmetry (Ψ_h) against ratio of bedload and suspended load transport in the upstream channel, and (c) Scatter plot ratio of bedload and suspended load transport in the upstream channels against the dominance of river flow over tidal flows in the upstream channels. The legend for all panels is provided in panel c.

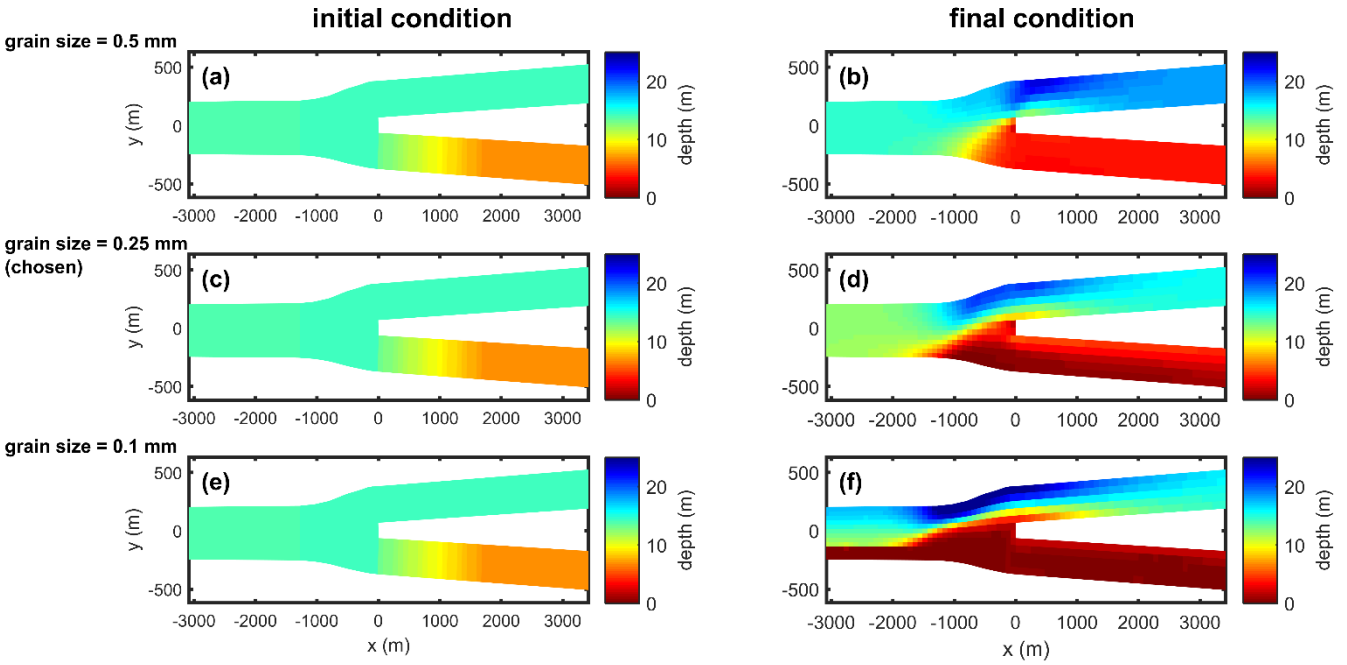

Figure 12: Initial (a, c, and e) and final (b, d, and f) depth near the bifurcation for coarser sand (a and b), applied sand (c and d), and finer sand (e and f) using the set-up of simulation Depth1_Q2800.

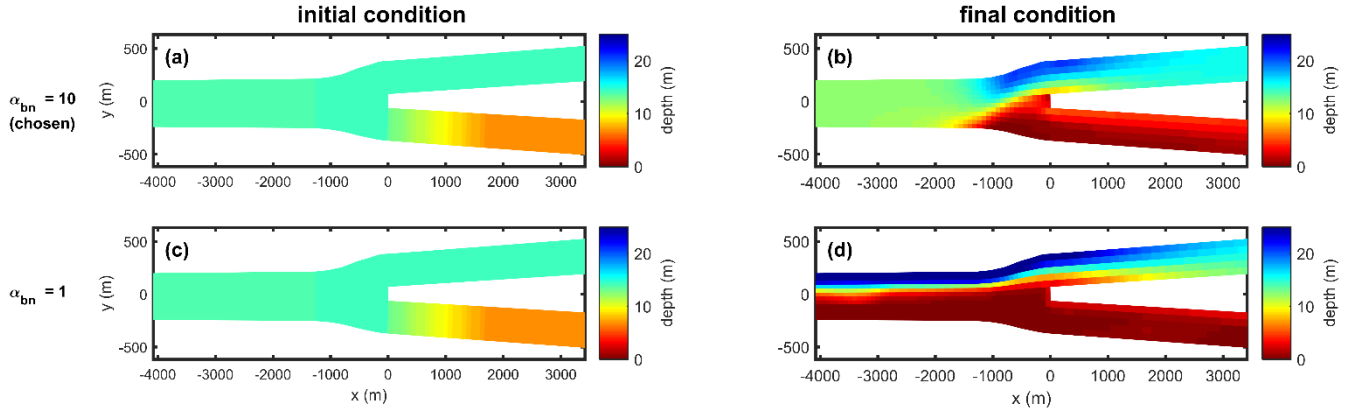

Figure 13: Initial (a and c) and final (b and d) depth near the bifurcation for large (a and b) and small (c and d) α_{bn} using the set-up of simulation Depth1_Q2800.

Appendix A

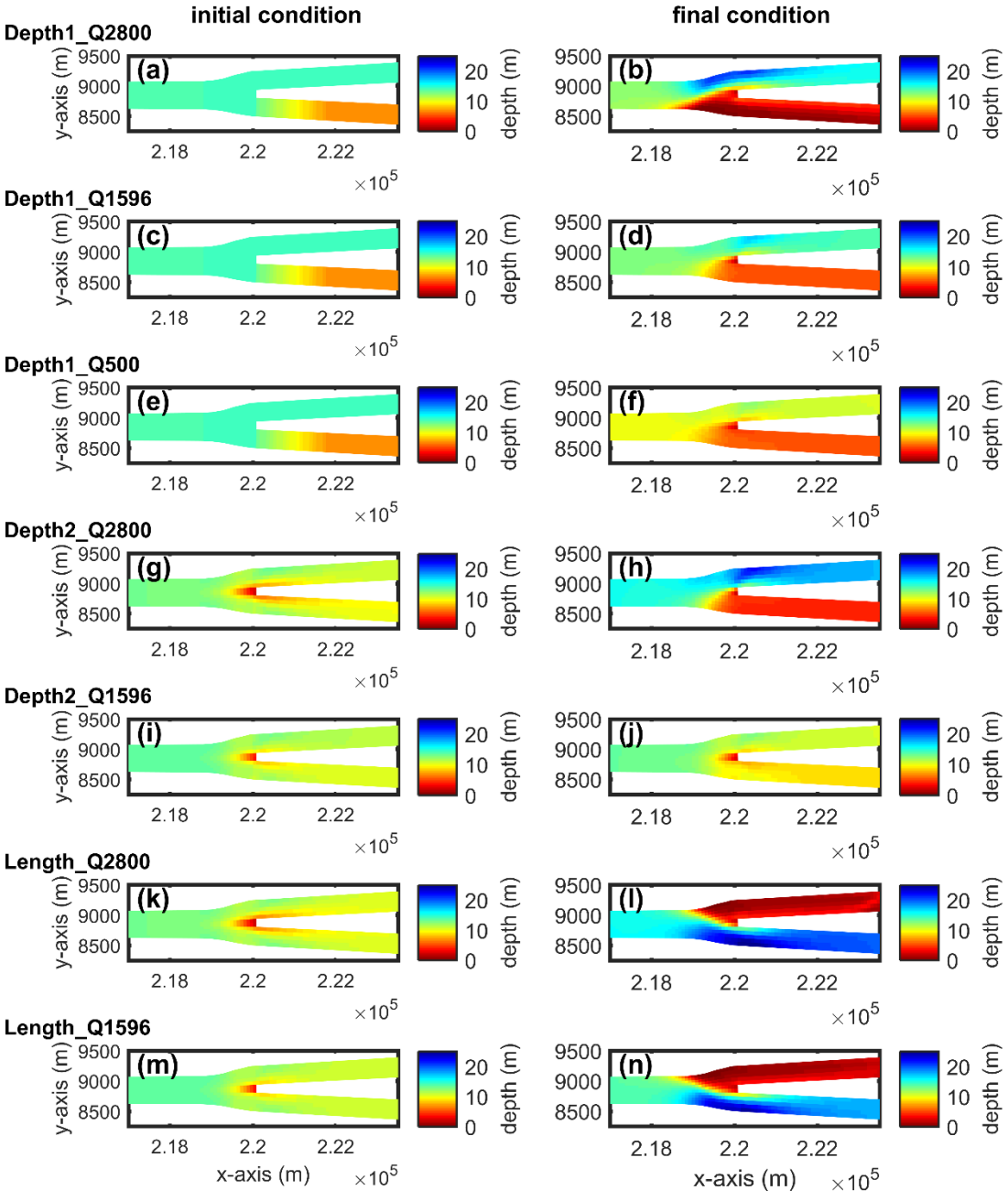
initial condition
final condition
Depth1_Q2800
Depth1_Q1596
Depth1_Q500
Depth2_Q2800
Depth2_Q1596
Length_Q2800
Length_Q1596
(a)
(b)
(c)
(d)
(e)
(f)
(g)
(h)
(i)
(j)
(k)
(l)
(m)
(n)
y-axis (m)
9500
9000
8500
2.18
2.2
2.22
×10^5
x-axis (m)
depth (m)
20
10
0

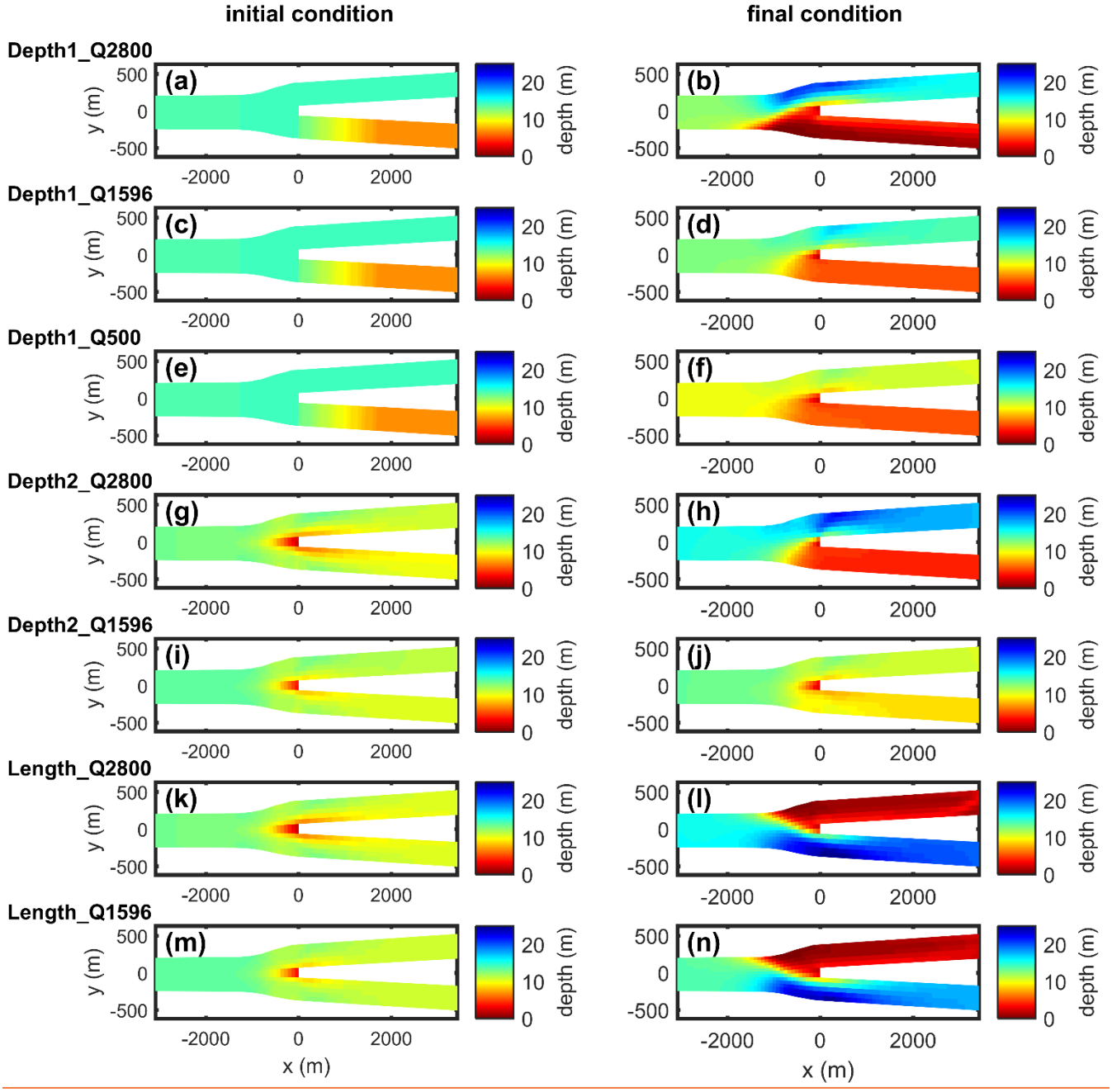

610 **Figure A1: Initial (left panels) and final (right panels) depth near the bifurcation for all simulations in Case 1. For Depth difference scenario (panel a-j), the top branch in each panel is the deep downstream branch and the bottom one is the shallow downstream branch. For Length difference scenario (panel k-n) the top branch in each panel is the long downstream branch and the bottom branch is the short downstream branch.**

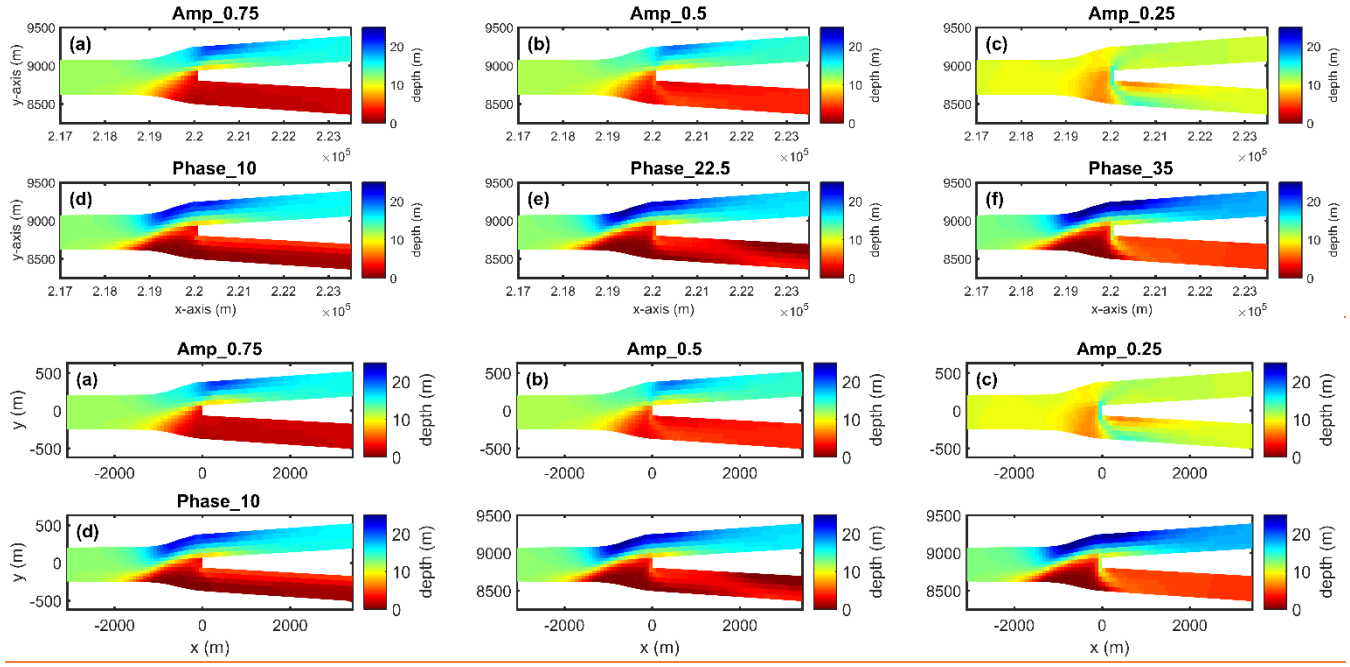

Figure A2: Final depth for Case 2. For amplitude difference scenario (panel a-c) the downstream branch imposed by low tides is the bottom branch while for phase difference scenario (panel d-f) the bottom branch is the downstream branch imposed by delayed tides.

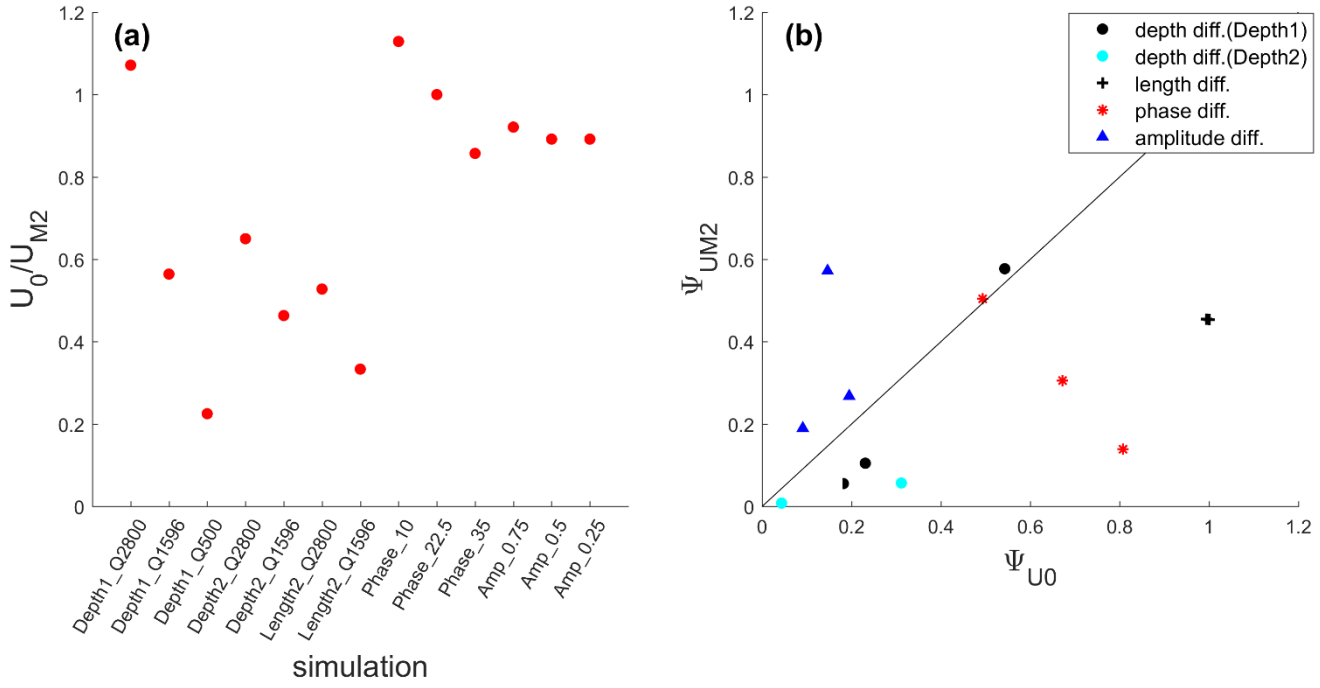

Figure A3: (a) Ratio of U_0 and U_{M2} for all simulations and (b) Comparison of asymmetry of U_{M2} against asymmetry of U_0.

Table A1: sediment mobility (tide-averaged and maximum), mean flow and tidal flow amplitude at the cross sections near the bifurcation as shown in Figure 2 for all simulations. Main channel is the upstream channel, minor channel is the downstream channel that tend to be shallower, and major channel is the deepened downstream channel.

Simulation	Mobility (τ_{*ave})			Mobility (τ_{*max})			U_0			U_{M2}		
	main channel	minor branch	major branch	main channel	minor branch	major branch	main channel	minor branch	major branch	main channel	minor branch	major branch
Depth1_Q2800	0.76	0.04	0.28	0.66	0.14	0.67	0.30	0.16	0.54	0.28	0.14	0.52
Depth1_Q1596	0.28	0.09	0.16	0.29	0.24	0.44	0.22	0.20	0.32	0.39	0.42	0.52
Depth1_Q500	0.07	0.07	0.09	0.20	0.18	0.26	0.09	0.09	0.13	0.40	0.45	0.50
Depth2_Q2800	0.13	0.10	0.19	0.37	0.29	0.50	0.26	0.21	0.40	0.40	0.45	0.50
Depth2_Q1596	0.10	0.11	0.12	0.27	0.30	0.31	0.19	0.22	0.24	0.41	0.49	0.50
Length2_Q2800	0.11	0.02	0.22	0.31	0.08	0.60	0.19	0.00	0.44	0.31	0.20	0.53
Length2_Q1596	0.08	0.02	0.15	0.24	0.08	0.45	0.12	-0.01	0.29	0.32	0.21	0.55
Phase_10	0.15	0.04	0.28	0.40	0.16	0.67	0.30	0.18	0.53	0.31	0.17	0.55
Phase_22.5	0.15	0.04	0.28	0.38	0.16	0.66	0.26	0.10	0.51	0.36	0.30	0.56
Phase_35	0.17	0.07	0.27	0.41	0.20	0.68	0.22	0.05	0.47	0.45	0.47	0.61
Amp_0.75	0.17	0.10	0.26	0.42	0.23	0.66	0.35	0.35	0.47	0.31	0.16	0.58
Amp_0.5	0.19	0.11	0.26	0.49	0.37	0.66	0.33	0.31	0.46	0.40	0.35	0.61
Amp_0.25	0.23	0.20	0.25	0.54	0.58	0.59	0.33	0.42	0.35	0.51	0.49	0.71